11. Kirkendall Analysis and the Effect of Annealing Temperature on the Leak Formation and Long-Term Stability of Composite Pd/Ag Membranes

11.1. Introduction

The leak formation in composite Pd membranes results in a gradual decline in the H_2/He selectivity as a function of time and alters the long-term stability. The leak growth in pure Pd membranes has been shown to be significant at temperatures above 400-450°C (Guazzone, 2005). Among possible mechanisms that led to the formation of leaks, in comparison with the release of thermal and hydrogen stresses at or above 400°C, the incoherent sintering of Pd crystallites in H_2 atmosphere above 400°C appeared to be the most dominant processes. In addition, the straightening of the grain boundary network due to grain boundary migration at 500°C was shown to be faster in H_2 and argued as a possible mechanism for the leak formation in composite Pd membranes (Saini, 2006).

Since high annealing temperatures are required to form the Pd/Ag alloy, the effects of the incoherent sintering and grain growth on the leak formation and growth have been a greater challenge for the composite Pd/Ag membranes. Unlike pure-Pd membranes, both

the formation and growth of the leak for Pd/Ag membranes arise at lower temperatures due to the low Tamman temperature and the high surface mobility of the Ag metal.

The main objective of this chapter was to evaluate the formation and the growth of the leak in composite Pd/Ag membranes during high temperature annealing of the as-synthesized Pd/Ag layers to form the Pd/Ag alloy. In addition, Pd/Ag alloy nanoparticles, which were synthesized at room temperature by a chemical reduction method, were used to form a uniform Pd/Ag alloy layer for the synthesis of Pd/Ag membranes 016 and 017. The effect of Pd/Ag alloy nanoparticles on the long-term stability and the leak growth was discussed in detail.

11.2. Effect of High Temperature Alloying on the Leak Development

To evaluate the leak characteristics during the annealing, a 37 μm thick Pd/Ag membrane 010 was prepared on a 0.2 μm media grade PSS support. The formation of the leak was monitored in a helium atmosphere from room temperature to 600°C. The helium permeance as a function of temperature and elapsed time is given in Figure 11-1.

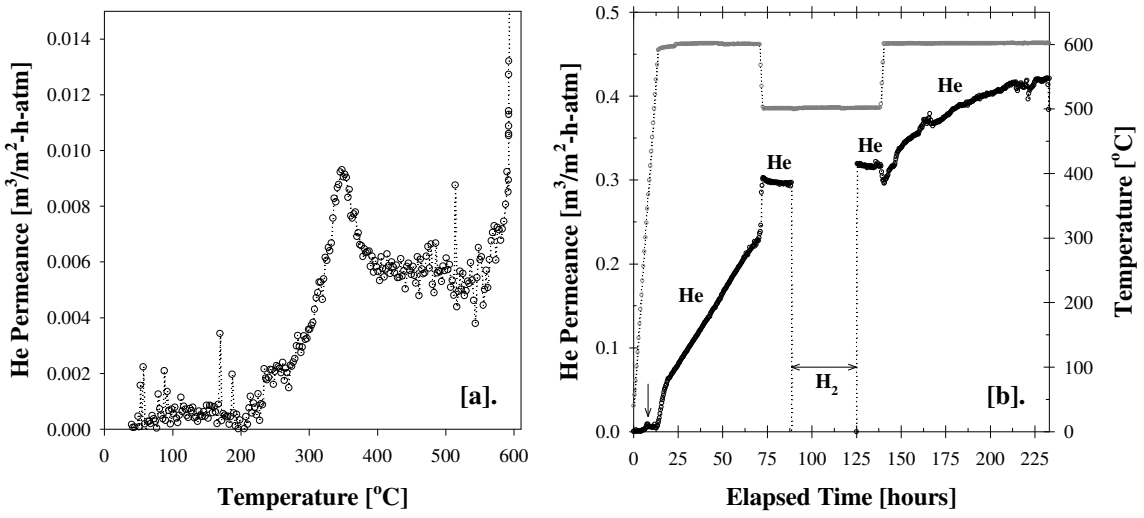

Figure 11-1: Leak development in the Pd/Ag/PSS membrane 010 [a].As a function of temperature during the initial heating in He and [b]. As a function of time at all temperatures

As can be seen in Figure 11-1[a], a first noticeable increase in He leak during the initial heating of membrane 010 occurred at a temperature range of 250-400°C, which corresponded to the first 5-10 hours of testing (region annotated by an arrow in Figure 11-1[b]). The increase in He leak during the initial heating period at relatively lower temperatures (250-400°C) might be attributed to the contribution of different processes. These include the presence of volatile chloride impurities, Pd and/or Ag oxides, the absorbed H_2O and the remnants of Sn and Na from $SnCl_2$ and Na_2EDTA used in the activation and plating solutions, respectively. While the absorbed H_2O between the deposition layers due to improper drying might have contributed to the leak formation, the presence of the chemical impurities (i.e., Sn, Na etc.) and their effect on the leak growth at lower temperatures might be of greater concern if the sample is not rinsed thoroughly.

Although XPS analysis of the freshly deposited Pd by Saini (2006) indicated no volatile chloride impurities, PdO was found to be present at the nanoscale level. Similar analyses are needed to evaluate the presence of chlorides and/or surface oxides for the freshly deposited Ag films. A list of possible oxides and chlorides within the temperature range of 100-460°C is given in Table 11-1.

Table 11-1. Thermal properties of different oxides and chlorides

	Color	Melting Point
CrO_2	Black	~400°C (loses O_2)
CrO_3	Dark red	190-197°C
$FeCl_2.2H_2O$	Very pale green	120-150°C (dehydrates)
$FeCl_2.4H_2O$	Pale green	105°C (dehydrates)
$FeCl_3$	Brown-black/green	306°C
AgO	Grey	>100°C (decomposes to Ag and O_2)
Ag_2O	Black/brown black	460°C
AgCl	White	455°C
PdO_2	Dark red/black	200°C (decomposes to PdO*)

Moreover, the grain growth of the as-synthesized Pd and Ag layers and the increase in dislocation density due to the re-arrangements of the grain boundaries might be a relativly important in contributing to the formation of leaks.

* PdO is black/green black in color and stable up to 750°C

A similar step changes in the He leak growth at lower temperatures (<400°C) were also observed for several other Pd/Ag membranes (i.e., 002, 007 (Ma-33) and 020). It is also interesting to note that the maximum in the He leak in Figure 11-1[a] was in close proximity to the Tamman temperature of Ag (344°C), indicating that the diffusion of Ag might also have caused in the formation of leak in the temperature range of 250-400°C.

The initial helium leak of the membrane after the step change at~ 350°C between 400°C and 500°C was 0.006 m^3/m^2-h-atm, shown by the arrow mark on Figure 11-1[b]. By the time the annealing temperature reached 600°C, a steady increase in the helium leak was monitored between 14 and 72 hours. The leak rate after 72 hours of annealing was 0.26 m^3/m^2-h-atm. This value was two orders of magnitude greater than the leak rate measured during the initial heating between 400°C and 500°C.

The possible physical causes for the progressive growth of the leak at 600°C were the formation of voids/openings at the cluster boundaries during cluster sintering and the deterioration of the dense Pd/Ag layer due to the high surface mobility of Ag. It should be also noted that the annealing temperature 600°C was well above the Tamman temperature of Ag metal and very close to that of Pd metal (640°C). Indeed, the SEI micrographs in Figure 5-8[e] (Column C4) clearly showed that the annealing temperature 600°C was high enough to result in a significant cluster sintering within layers.

To see the effect of lower annealing temperature on the leak growth, the membrane was cooled to 500°C. The helium leak rate at 500°C was 0.30 m^3/m^2-h-atm and was found to be quite stable for a period of 18 hours (between 72 and 90 hours in Figure 11-1[b]). The H_2 permeance of Pd/Ag/PSS membrane 010 at 500°C was 6.2 m^3/m^2-h-$atm^{0.5}$ between 90 and 115 hours (H_2 region shown in Figure 11-1[b]). The H_2 permeance at 500°C increased by 7% over the period tested. After switching back to helium, the leak of the membrane was measured for an additional 26 hours at 500°C (between 115 and 140 in Figure 11-1[b]) and found to be stable at a value of 0.32 m^3/m^2-h-atm. Since the helium leak after the H_2 permeance measurement was very similar to the value observed just prior to admitting H_2, the increase in H_2 permeance might be related to the continuation of the alloying of Pd and Ag. Nevertheless, the change in annealing

atmospheres from He to H_2 at 500°C did not result in a significant leak growth compared to the effect of temperature for this specific case. Finally, the membrane was heated to 600°C to monitor the development of the membrane leak for an additional 95 hours (between 140 and 235 hours in Figure 11-1[b]). The helium leak rate monitored during this period suggested further cluster sintering, similar to the steady leak development observed at 600°C between 14 and 72 hours. The helium leak rate was as high as 0.42 m^3/m^2-h-atm at the end of 235 hours of annealing, indicating the significance of the cluster sintering between Pd and Ag layers at 600°C.

The annealing treatment of the Pd/Ag/PSS membrane 010 indicated that the temperature had a significant effect on the leak development. This was particularly true at 600°C, where significant cluster sintering was also observed by the coupon studies (Figure 5-8[e]-C4), suggesting a possible relationship between leak development and cluster sintering. The process of cluster sintering may lead to the formation of small voids at the cluster boundaries, which eventually combine and grow to form through-through pinholes in the membrane layer. However, the pinhole formation for the annealed Pd/Ag layers was not visible on SEI micrographs compared to that of pure Pd layers annealed at the same temperature (Guazzone, 2005). It should be also noted that the the growth of the Ag clusters at 600°C (Figure 7-11[c] and Figure 8-5[b]) might have a significant contribution on the progressive growth of the leak.

Although temperatures lower than 600°C may result in the incomplete alloy formation, the progressive growth of the leak during the annealing of membrane 010 suggested that, mild annealing temperatures with longer time duration may be needed to alleviate the leak development.

11.3. Synthesis of Pd/Ag Alloy Nanoparticles

To avoid leak formation upon high temperature annealing, the preparation of nano-cyrstalline Pd/Ag alloy particles was investigated as an alternative synthesis route.

Among several different approaches of nanoparticles (NP) synthesis in the literature (Silvert *et al.*, 1996; Huang *et al.*, 1998; Damle *et al.*, 2002), the methodology outlined by

Huang *et al.* (1998) was preferred for its simplicity. The Pd and Ag precursors used for the synthesis of Pd/Ag alloy nanoparticles were $Pd(NO_3)_2$ and $AgNO_3$, respectively. After dissolving desired stoichiometric amounts of $Pd(NO_3)_2$ and $AgNO_3$ salts to prepare a Pd/Ag mixture with 25-30 wt% Ag, in DI H_2O with continuous stirring, 5 ml of 37% formaldehyde was added. Then, the required amount of concentrated NaOH solution (3M) was added until the solution became transparent with the formation of Pd/Ag nanoparticle colloids. In this particular case, formaldehyde and concentrated NaOH were used as the stabilizer and the reducing agent, respectively. Oswald Ripening was the growth mechanism where small particles dissolved, and were consumed by larger particles. One of the key aspects for the nanoparticle synthesis was to achieve fast nucleation and slow growth. In other words, particles had to be protected from Oswald Ripening by the use of stabilizers. Therefore, the role of stabilizers was to prevent uncontrollable growth and the aggregation of particles and to control the growth rate and particle size.

The colloids were agglomerated by the addition of acetone (3:1 by volume) and separated by filtering. Finally, Pd/Ag colloids were dried at 120°C overnight. The synthesis route that would lead to the formation of Pd/Ag alloy nanoparticles having a core-shell configuration is schematically shown in Figure 11-2.

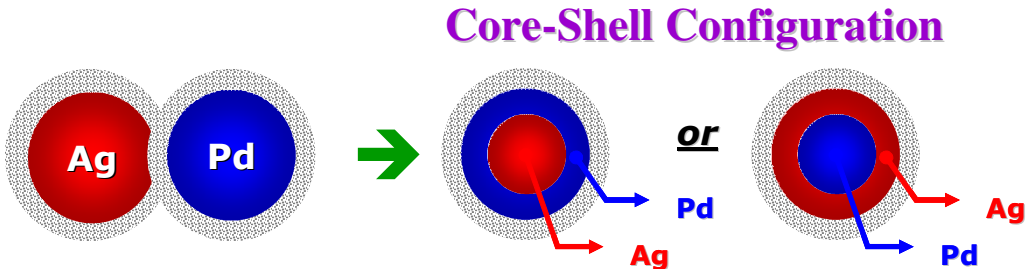

Figure 11-2: The formation of Pd/Ag alloy nanoparticles by the chemical reduction method

A comparison between as-synthesized Pd/Ag alloy nanoparticle powder and the Ag layer formed by the regular electroless plating on PHST coupon is shown in Figure 11-3. In comparison to the Ag deposit from a regular electroless plating bath, the SEI micrograph in Figure 11-3 indicated that the morphology of the as-synthesized powder consisted of very fine features.

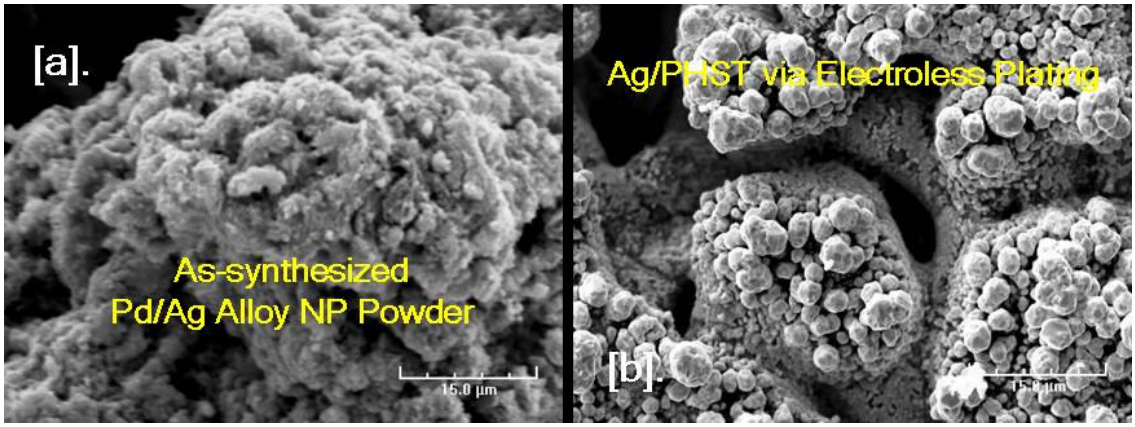

Figure 11-3: SEI micrographs for the [a]. As-synthesized Pd/Ag alloy nanoparticle powder (mounted on top of aluminum sample holder by the use of carbon paint) and [b]. Ag on an un-oxidized PHST coupon via regular electroless plating

Furthermore, EDX area scans on the Pd/Ag alloy nanoparticle powder indicated a composition range of 29-32 wt% Ag and 65-66 wt% Pd, with trace amounts of impurities. This was also in good agreement with the selected synthesis stoichiometry in order to achieve Pd/Ag alloy nanoparticles with the Ag content in the range of 25-30 wt%. EDX spectrum of the Pd/Ag alloy nanoparticles is shown in Figure 11-4.

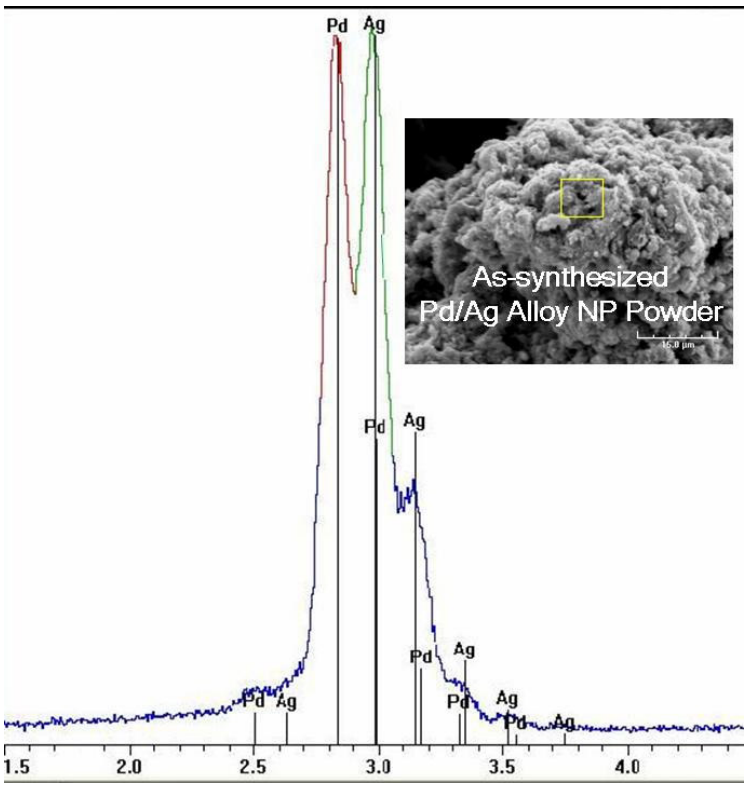

Figure 11-4: EDX spectrum for the Pd/Ag alloy nanoparticles. Inset SEI micrograph shows the as-synthesized Pd/Ag alloy NP powder

The X-ray diffraction pattern, shown in Figure 11-5[d], clearly indicated that the as-synthesized powder had a fcc Pd/Ag alloy phase, with an average particle size of 3.7 nm, which was determined by the Scherrer formulation (Cullity and Stock, 2001). This was an order of magnitude smaller than the average particle size (38.5 nm) of a Pd/Ag alloy layer formed by the electroless plating and after annealing at 600°C in He for 10 hours, shown by the XRD pattern given in Figure 11-5[c]. This was taken as the direct evidence that the synthesized powder by the use of chemical reduction method led to the formation of Pd/Ag alloy nanoparticles at room temperature.

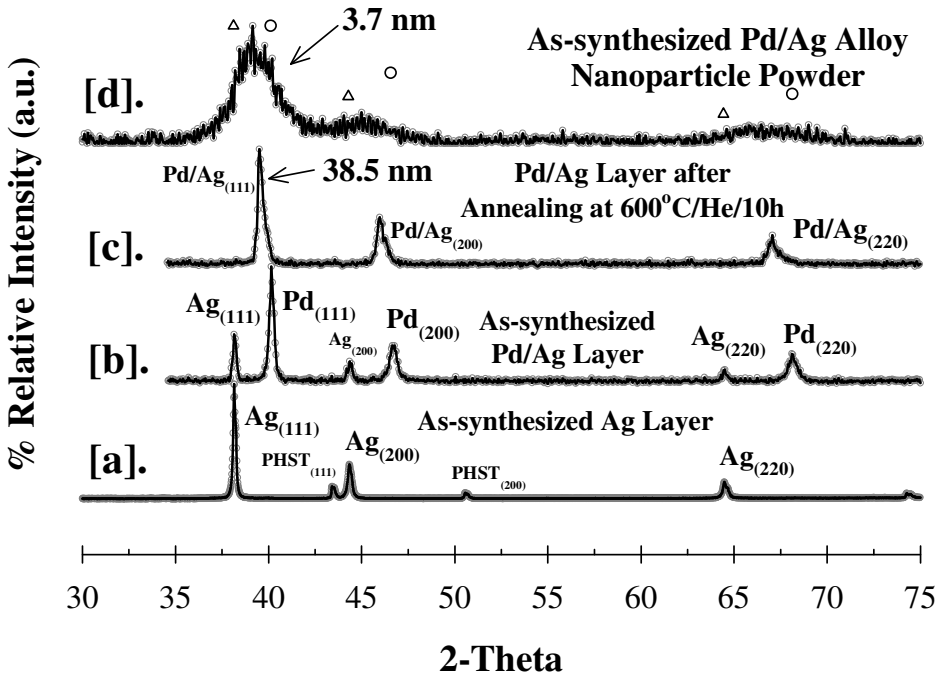

Figure 11-5: XRD patterns for the [a]. pure-Ag layer formed by electroless plating, [b]. Pd and Ag layers formed by electroless plating, [c]. Pd/Ag alloy phase formation upon annealing of the as-synthesized Pd/Ag layer at 600°C/He/10h and [d]. As-synthesized Pd/Ag alloy nanoparticle

The alloying of bimetallic nanoparticles take place at lower temperatures due to the fact that the driving force for the coalescence of two nanoparticles was the reduction in the free energy through a reduction in the surface area. For instance, a small metal nanocrystal of 1 nm diameter will have ~100% of its atoms on the surface. On the other hand, the percentage of surface atoms for a metal nanocrystal of 10 nm diameter is approximately around ~15%. Indeed, the lower temperature alloying of bimetallic nanoparticles would be possible since the melting temperature and the latent heat of fusion are dependent on the particle size and are markedly lower than those of their bulk counterparts.

If a uniform continuous layer of Pd/Ag alloy nanoparticles could be successfully formed on a porous support surface prior to the formation of a final dense Pd layer, it would be possible to avoid conventional high temperature diffusion treatment to form the Pd/Ag alloy. A layer of Pd/Ag alloy nanoparticles might help reduce the formation of progressive leaks since annealing temperatures as high as 600°C for the sintering between large Pd and Ag clusters formed by electroless plating could be avoided. The presence of a Pd/Ag alloy nanoparticle layer might further enhance the H_2 permeance.

11.4. The Effect of Pd/Ag Alloy Nanoparticles on H_2 Permeance, Leak Stability and Membrane Morphology

In order to investigate the effect of Pd/Ag alloy nanoparticles on low temperature sintering of metal clusters, H_2 permeance and leak formation, uniform layers of Pd/Ag alloy nanoparticles were dip coated from a nanoparticle slurry under vacuum suction during the synthesis of membranes 016 and 017. The Pd/Ag alloy NP solution was prepared by mixing 0.5033g of Pd/Ag NP powder in 150 mL DI H_2O. A stable slurry was formed after keeping the NP solution in ultrasonic bath for 30-60 minutes.

The supports used for the synthesis of the membranes were 0.1 μm media grade, ½" OD and 2" long Inconel tubes, which were oxidized at 800°C for 12 hours. The $Al(OH)_3$ grading and the deposition of the pure-Ag barrier layer for the membranes 016 and 017 were performed similar to the synthesis procedure illustrated in Figure 8-8[a] and [b],

respectively. The synthesis history for membranes 016 and 017 are shown in Figure 11-6. While the NP layer for membrane 016 was dip coated immediately after the $Al(OH)_3$ grading layer and stabilized with 30 minutes of Pd plating prior to pure-Ag barrier layer, the NP dip coating layer for membrane 017 was formed after the the $Al(OH)_3$ grading and the deposition of the pure-Ag barrier layer, as shown in Figure 11-6.

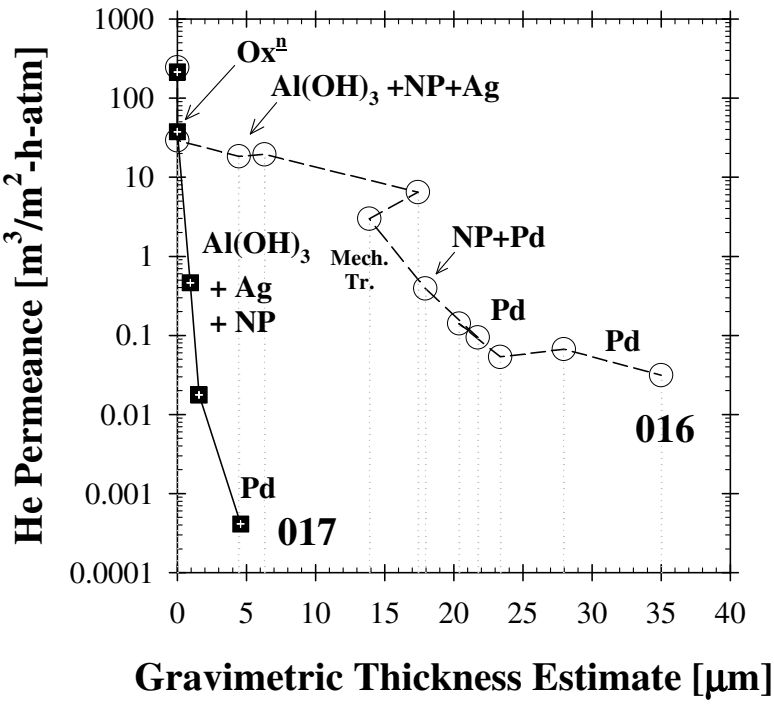

Figure 11-6: Synthesis history for the membranes 016 and 017

As can be seen in Figure 11-6, the synthesis of membrane 016 required additional electroless Pd plating steps in order to achieve a gas tight layer. The final thickness and the Ag content of membrane 016 were gravimetrically estimated as 35 μm and 4.6 wt%, respectively. On the other hand, the final thickness and the Ag content of membrane 017 were as thin as 4.6 μm and as high as 31.3 wt%, respectively, as shown in Figure 11-6.

The H_2 permeance for membranes 016 and 017 are compared at 350°C and 500°C as shown in Figure 11-7[a] and [b], respectively.

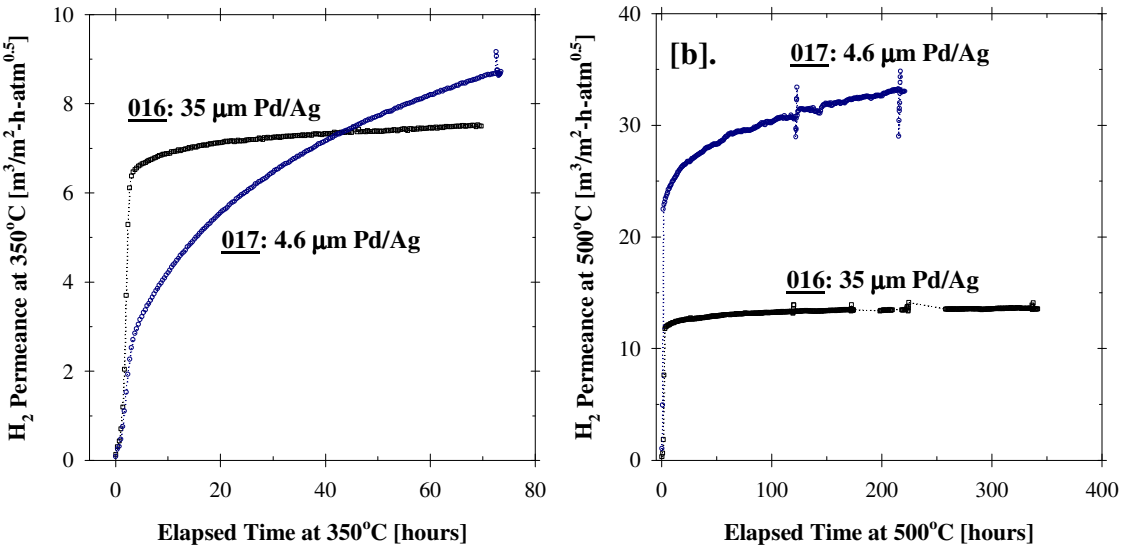

Figure 11-7: H_2 permeance for membranes 016 and 017 as a function of time at [a]. 350°C and [b]. 500°C

At 350°C, the H_2 permeance for membranes 016 and 017 after a total testing period of 72 hours were 7.4 and 8.7 m^3/m^2-h-$atm^{0.5}$, respectively, as shown in Figure 11-7[a]. Figure 11-7[a] shows that due to the close proximity to the Tamman temperature of Ag, the steady increase in the H_2 permeance of the 4.6 µm thick Pd/Ag membrane 017 at 350°C suggested a possible alloying effect due to the diffusion of Ag in the Ag-rich layer (31.3 wt% Ag) into the top Pd layer. In contrast, the stable H_2 permeance of the 35 µm thick Pd/Ag membrane 016 was also attributed to the Ag content, which was too low (4.6 wt%) to result in an enhancement in H_2 permeance.

Similar trends in H_2 permeance was also observed at 500°C as shown in Figure 11-7[b]. The H_2 permeance for membranes 016 and 017 at 500°C were 13.7 (~340 hours) and 35.7 (~215 hours) m^3/m^2-h-$atm^{0.5}$, respectively. However, the H_2/He selectivity of the 35 µm and 4.6 µm thick Pd/Ag membranes 016 and 017 were below ~100 and even below ~20 after testing at 350°C and 500°C, respectively. Compared to the annealing temperature of membrane 010 (600°C), annealing of the Pd/Ag layers at a temperature 500°C was relatively too low to initiate significant cluster sintering. Indeed, it was way below the Tamman temperature of Pd. However, the leak rates measured for membranes 016 and 017 were extremely high. The final room temperature helium permeance for membranes 016 and 017 were ~0.6 and as high as ~6.0 m^3/m^2-h-atm, respectively. Since

such high leak rates might indicate the presence of cracks and/or macroscopic defects within the membrane layer, both membranes were cut, mounted and surface polished for detailed SEI and EDX analyses in order to investigate the possible cause of the leak formation. The cross-sectional SEI micrographs for membranes 016 and 017 are shown in Figure 11-8.

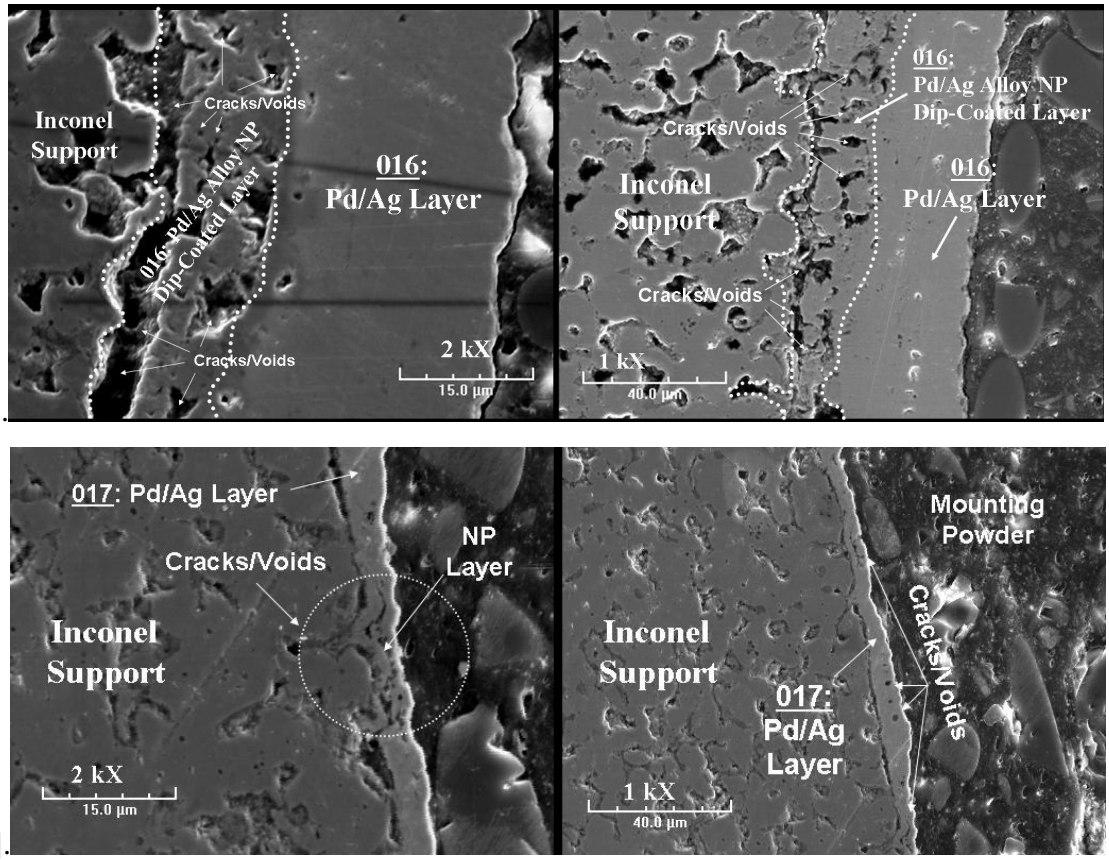

Figure 11-8: Cross-sectional SEI micrographs for the membranes [a]. 016 and [b]. 017 at different magnifications

As can be depicted in Figure 11-8[a], the original interface between the porous metal support and Pd stabilized Pd/Ag alloy NP layer appeared to form large cracks and voids during the long-term H_2 permeation test over a temperature range of 250-500°C. It was also interesting to note in Figure 11-8[a] that there was a clear transition between the top Pd/Ag layer and the layer identified with the formation of large cracks and voids. Indeed, the Pd stabilized Pd/Ag alloy NP layer in Figure 11-8[a] appeared to look almost detached from the porous metal support interface and resembled to that of a diffusion zone. Therefore, the formation of large cracks and voids at the interface, shown in Figure

11-8[a], was attributed to the diffusion that took place at 500°C between the original NP layer and the top Ag and Pd layers, which appeared to erode the compactness of the entire Pd/Ag layer. The formation of a progressive He leak and a dramatic decline in H_2/He selectivity for membrane 016 was also in good agreement with the SEI micrographs shown in Figure 11-8[a].

Similarly, the cross-sectional SEI micrographs shown in Figure 11-8[b] for the membrane 017 indicated the presence of large cracks and voids, corresponding to the region which was originally dip coated with the Pd/Ag alloy NP, as shown in Figure 11-6. The SEI micrographs in Figure 11-8[b] suggested that the effect of interdiffusion within the region that was originally dip coated with the Pd/Ag alloy NP layer might be significantly higher on the leak development due to the thinness of the composite Pd/Ag layer (4.6 μm). Indeed, the final room temperature He permeance for membrane 017 was an order of magnitude higher than that of membrane 016. As conclusively shown by the cross-sectional SEI micrographs in Figure 11-8[a] and [b], the morphology for both membranes were severely altered by the dominant presence of the Kirkendall voids and/or porosity.

The Kirkendall porosity occurs when the diffusing rates of two or more elements are not the same (i.e., $D_A \neq D_B$). In other words, the Kirkendall effect (Kirkendall *et al.*, 1939; Kirkendall, 1942; Smigelskas and Kirkendall, 1947) stems from the difference in individual diffusion mobility between the elements of diffusion couple (Höglund and Agren, 2001). The self and/or tracer and/or intrinsic diffusion coefficients for Ag and Pd at 500°C are 1.3×10^{-17} m^2/s and 2.1×10^{-23} m^2/s, respectively (Brandes and Brook, 1998). Such a difference in the self-diffusion coefficients of Ag and Pd usually results in the formation of a concentration gradient. Since the conservation of lattice sites requires equal atomic fluxes according to Kleppa (1955), the presence of such an uncompensated diffusion results in the formation of a vacancy flux, which is also termed as the "vacany wind" (Seizt, 1948). As pointed out by Van Dal *et al.* (2000), the Kirkendall effect, often accompanying interdiffusion in solids and mainly in FCC systems, manifests itself in various phenomena such as migration of macroscopic inclusions inside the diffusion zone, the development of diffusional porosity, the generation of internal stress and even

deformation of the material on a microscopic scale. The progressive leaks observed for membranes 016 and 017 were qualitatively in good agreement with these observations.

The alloying of bimetallic nanoparticles took place at lower temperatures due to the fact that the driving force for coalescence of two nanoparticles was the reduction in the free energy through a reduction in the surface area. Since the particle size markedly affected the melting temperature and the latent heat of fusion, the diffusion rates of the as-synthesized Pd/Ag alloy nanoparticles were expected to be higher than those of their bulk counterparts (i.e., Ag and Pd formed by the electroless plating). Indeed, experiments conducted by Nachtrieb *et al.* (1957) suggested that the diffusion coefficient of Ag in Pd was a linear function of a temperature ratio of type T_m/T, where T_m and T are the melting and annealing temperatures in K, respectively, and expressed as follows:

$$D_{Ag\to Pd}\left(\frac{m^2}{s}\right) = 2.7\times10^{-5}\, e^{-17.75\frac{T_m}{T}} \qquad (11\text{-}1)$$

Since the density of the mobile lattice vacancies depended upon the temperature ratio T_m/T, Nachtrieb *et al.* (1957) further postulated that the diffusion and melting were linked through the T_m/T, in which the melting occurred when the density reached a critical value. Based on the above hypothesis and by the use of Equation (11-1), at an annealing temperature of 500°C, the self-diffusion coefficient estimates for Ag (T_m=960°C) and the Pd/Ag alloy NP (T_m=120°C) in Pd were $4.3\text{x}10^{-20}$ m^2/s and $3.8\text{x}10^{-7}$ m^2/s, respectively. The estimated self-diffusion coefficient for the Pd/Ag alloy nanoparticles at 500°C were in the same order of magnitude as the grain boundary diffusion coefficients of Ag, which were reported as $1.3\text{x}10^{-7}$ m^2/s (Hoffmann and Turnbull, 1951) and $6.5\text{x}10^{-7}$ m^2/s (Smoluchowski, 1952). Therefore, the Kirkendall porosity formed in the Pd/Ag alloy NP layers of membranes 016 and 017 (shown in Figure 11-8[a] and [b]), was due to noticeably fast diffusion coefficients expected for the nanoparticles. In the proximity or above the melting point of nanoparticles, the amount of thermal vacancies increased with the enhancement of atomic mobilities both for bulk Ag metal and the Pd/Ag alloy nanoparticles. This generated a greater driving force for the formation of Kirkendall voids and thus resulted in progressive leaks and the deterioration of the H_2/He selectivity for membranes 016 and 017.

As can be depicted from the SEI micrographs in Figure 11-9 the annealed morphology of the membrane 016 appeared to have larger grains and/or clusters compared to the smaller clusters with finer grains for membrane 017. Since the extent of the He leak for membrane 017 was an order of magnitude higher than that of 016, the diffusion of molecular H_2 through the cracks and voids in the Pd/Ag layer of membrane 017 is expected to be more pronounced. Therefore, coupled with the SEI micrographs shown in Figure 11-9, the extent of the He leak might also indicate a possible relationship with the growth of the Pd/Ag grains/clusters during annealing.

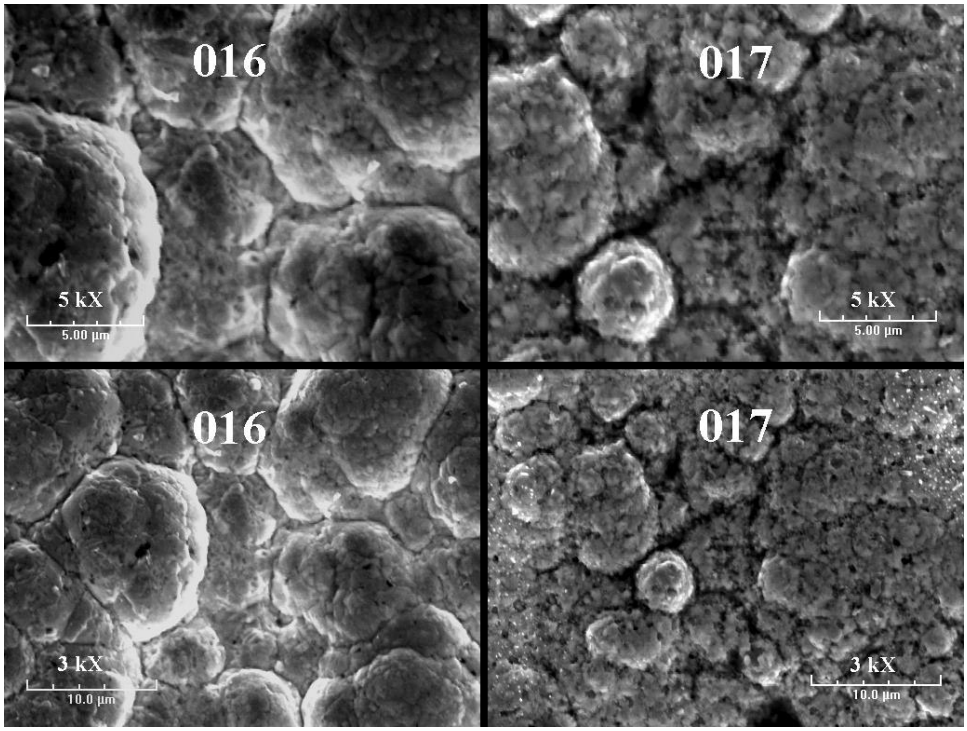

Figure 11-9: Top surface SEI micrographs for the membranes 016 and 017

The effect of annealing atmosphere on the microstructure and Pd/Ag alloy phase formation is further discussed via HTXRD temperature-ramp annealing of the as-synthesized Pd/Ag layers.

11.5. The Effect of Annealing Atmosphere and Temperature on the Formation of Kirkendall Voids/Porosity

In order the assess the role of the annealing atmosphere on the Pd/Ag alloy formation and its effect on the morphology, a 9.2 μm Pd/Ag (22.5 wt% Ag) and a 9.6 μm Pd/Ag (23.4 wt% Ag) layers were prepared on PHST coupons (oxidized at 800°C for 12 hours) by electroless plating and then annealed at a temperature range of 500-750°C in He and H_2 atmospheres, respectively. The temperature-ramp annealing of the Pd/Ag/PHST specimens via *in-situ* time-resolved HTXRD were carried out at 25°C intervals and for a period of 2 hours at each temperature over the range of 500-750°C.

The HTXRD 3D reaction pathway plots for the Pd/Ag/PHST samples annealed in H_2 and He are shown in Figure 11-10[a] and [b], respectively. In Figure 11-10[a], a sharp descend of the characteristic Ag peak and a significant increase in the Pd/Ag alloy phase at the (111) plane corresponded to the temperature range of 600-650°C. A further increase in the annealing temperature up to 750°C in H_2 resulted in a complete transformation of the Pd/Ag alloy phase as can be depicted in Figure 11-10[a]. On the other hand, the annealing in the helium atmosphere at the same temperature range resulted in a relatively more gradual transformation as shown in Figure 11-10[b].

The SEI micrographs shown in Figure 11-11[a] and [b] also indicated that the formation of the Pd/Ag alloy phase resulted in a significant cluster sintering of the as-synthesized Pd and Ag clusters. Similarly, the extent of cluster sintering for the Pd/Ag/PHST sample annealed in H_2 (Figure 11-11[a]) was in good qualitative agreement with the higher degree of transformation observed in Figure 11-10 [a].

Although the annealing temperatures as high as 750°C was tested, there were no visible pinhole formations on the surface of the Pd/Ag/PHST samples upon annealing in H_2 or He atmospheres (Figure 11-11[a] and [b]). It is however interesting to note that the H_2 annealing atmosphere had a substantial effect on the cross-sectional morphology compared to Pd/Ag/PHST sample annealed in helium. The cross-sectional SEI micrographs and the EDX line scans for the samples annealed in H_2 and He atmospheres are shown in Figure 11-12[a] and [b], respectively.

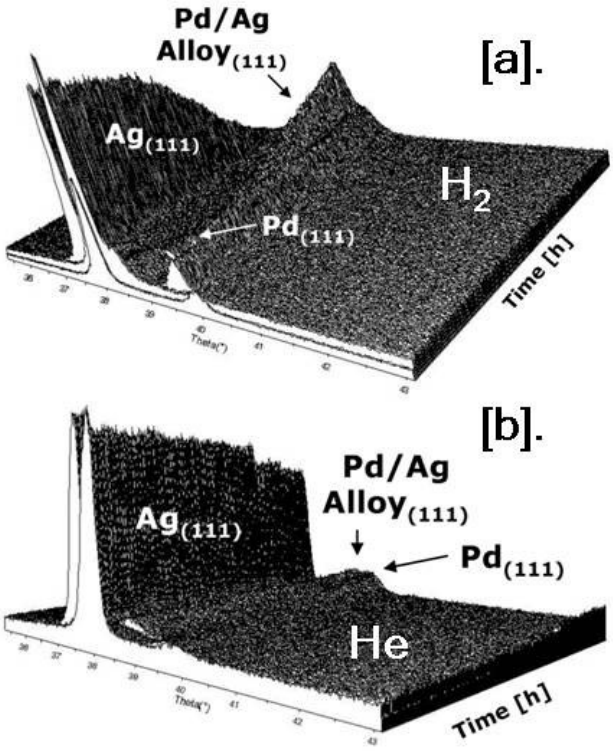

Figure 11-10: HTXRD 3D reaction pathway plots for the Pd/Ag/PHST samples annealed over a temperature range of 500-750℃ (25℃/step and 2 hours per temperature) in [a]. H_2 and [b]. He

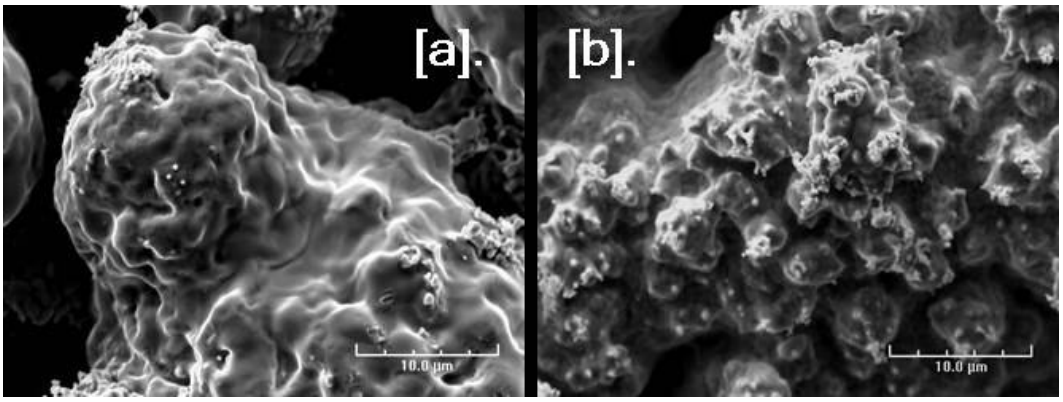

Figure 11-11: SEI top-surface morphology of the Pd/Ag/PHST samples after annealing over a temperature range of 500-750℃ in [a]. H_2 and [b]. He

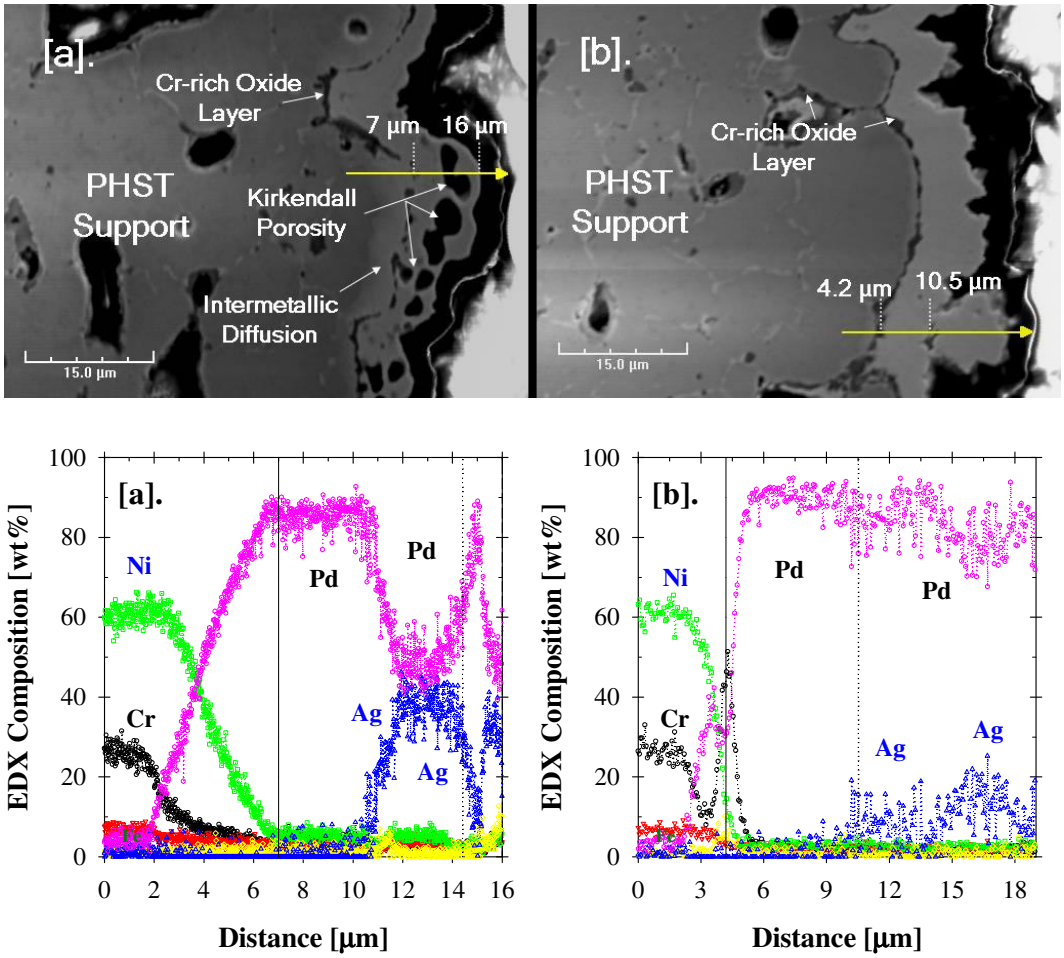

Figure 11-12: Cross-sectional SEI micrographs and the EDX line scans of the Pd/Ag/PHST samples after annealing over a temperature range of 500-750℃ in [a]. H_2 and [b]. He

It is clear in Figure 11-12[a] that the cross-sectional morphology or the Pd/Ag layer after annealing in H_2 over a temperature range of 500-750°C was dominated by the presence of Kirkendall voids of different shapes and sizes in the range of 3-9 µm. The average Ag content of the Pd/Ag alloy was ~40 wt%. It was also visible both in the SEI micrographs and the EDX line scan that the intermetallic diffusion led to the formation of a Pd-rich Pd/Ni alloy phase. However, the SEI micrograph also indicated that the Cr-rich oxide layer formed by the oxidation at 800°C was still present.

On the other hand, the annealing of the Pd/Ag/PHST sample in the He atmosphere as shown in Figure 11-11[b] led to the formation of neither Kirkendall porosity nor significant intermetallic diffusion at the interface. The average Ag content of the Pd/Ag alloy was ~20 wt%.

The temperature-ramp annealing of the Pd/Ag/PHST specimens via *in-situ* time-resolved HTXRD indicated that the formation of Kirkendall porosity mainly took place in the H_2 atmosphere. Since both Ag and atomic hydrogen compete for the 4d band of palladium, the dilation of the Pd lattice due to the presence of absorbed hydrogen appears to facilitate further Ag diffusion. However, the differences in the diffusion coefficients between Pd and Ag, ultimately led to the formation of the Kirkendall voids/porosity.

11.6. Conclusions

The formation of the leak was monitored for a 37 μm thick Pd/Ag/PSS in the helium atmosphere from room temperature to 600°C and over a period of ~215 hours. It was found that the leaks in Pd/Ag membranes started forming at a relatively low temperature range of 250-400°C followed by a progressive growth at temperatures higher than 500°C. Although the annealing temperatures as high as 600°C were required to form uniform Pd/Ag alloy layers, significant cluster sintering and the progressive growth of the leak was yet to be addressed.

In an effort to alleviate leak formation at high temperature annealing, Pd/Ag alloy nanoparticles with an average particle size of 3.7 nm were successfully synthesized at room temperature conditions and dip coated as uniform layers for the synthesis of membranes 016 and 017. The H_2 permeance testing of the composite Pd/Ag membranes having Pd/Ag alloy NP layers resulted in the formation of extremely high leak rates at 500°C.

The microstructure analysis of both membranes revealed the presence of cracks and voids at regions, which were originally dip coated with the nanoparticles. The formation of cracks/voids was identified as the Kirkendall porosity, which stems from the difference in individual diffusion mobility between the elements of diffusion couple. In this particular case, in contrast to having a leak mitigation effect, the use Pd/Ag alloy nanoparticles deteriorated the permselectivity of membranes 016 and 017.

According to the temperature-ramp annealing of the Pd/Ag/PHST specimens via *in-situ* time-resolved HTXRD, the Kirkendall porosity was only observed for the samples

annealed in the H_2 atmosphere. Coupled with the SEI micrographs and the EDX line scans, HTXRD analysis suggested that it might be necessary to conduct high temperature annealing of the as-synthesized Pd/Ag deposits in He atmosphere in order to avoid the formation of the Kirkendall porosity.

12. Conclusions

◊ The most significant improvement in membrane performance has been the increase in the safe operational temperature of the composite Pd/PSS and Pd/Alloy/PSS membranes to 500°C and above by the use of the porous Pd/Ag barrier formed by the bi-metal multilayer (BMML) deposition technique.

◊ The porosity of the Pd/Ag barrier layer in the BMML deposit was confirmed with the room temperature helium permeance measurements coupled with the SEI micrographs of the deposition morphology. In addition, the porosity of the Pd/Ag layer upon annealing was also stable at 500°C and above.

◊ Furthermore, the XRD phase identification and cross-section EDX line scan analyses showed that the Pd/Ag barrier layer formed an fcc Pd/Ag alloy phase upon high temperature annealing at 600°C.

◊ The porous Pd/Ag barrier was extremely effective as a barrier layer against intermetallic diffusion, which significantly improved the thermal and the long-term stability of the membranes for high temperature applications.

◊ Detailed microstructure analysis showed that the "Ag directed" electroless deposition morphology resulted in the non-uniform and heterogeneous rough surface coverage and led to the formation of 5-20 μm thick dendritic clusters that grew perpendicularly to the surface.

◊ The concept of blocking the large pores on the surface of the support metal by simply taking advantage of the dendritic growth characteristics of the Ag clusters

was successfully utilized via the Hole Blowing Technique (HBT) in order to form thin Ag-rich Pd/Ag layers and more importantly to avoid compositional variance within the Pd/Ag layers.

◊ Although HBT was not a surface modification technique, it was effective in partial blockage of the support pores as evidenced by the cross-sectional SEI micrographs.

◊ The final thickness of the composite Pd/Ag membranes prepared via the HBT were in the order of 15-25 μm with variable Ag content in the range of 2-20 wt% and H_2 permeance as high as 30 m^3/m^2-h-$atm^{0.5}$ at 500°C.

◊ The surface modification of the porous metal supports was mainly accomplished by the use of the $Al(OH)_3$ particles from a dense $Al(OH)_3$ slurry and applied at a reduced number of synthesis steps for the preparation of composite thin Pd and Pd/Ag membranes. The $Al(OH)_3$ grading procedure did not include any intermediate Pd and/or Ag plating to consolidate (glue) the powders

◊ The detailed FT-IR and XRD analyses showed that the phase transformation of the $Al(OH)_3$ from Gibbsite to Bohmite and to Akdalaite with the increasing temperature resulted in the formation of different crystal structures each exerting different physical properties. Indeed, ~60% of the support pores filled with the $Al(OH)_3$ powder transformed to a denser state at high temperatures (350-500°C).

◊ From the standpoint of support surface modification with the use of $Al(OH)_3$, and in comparison to the pre-activated Al_2O_3, ZrO_2, SiO_2 and CeO_2 particles, the effect of mass transfer resistance was expected to be less pronounced for $Al(OH)_3$ due to its low residual volume at high temperatures.

◊ The intermetallic diffusion induced alloy phases and the subsequent microstructure formation at the interface between the porous sintered metal supports (i.e., PSS, PHST, Inconel) and the Pd and Ag layers in the absence of a barrier layer was studied over a temperature range of 500-800°C in H_2 atmosphere.

◊ It was verified by the X-Ray phase analysis that Pd formed completely miscible solid solutions with both Fe and Ni after annealing in H_2 over a temperature range of 500-800°C. In contrast, the solid-phase immiscibility of the Ag metal with the support metals in the temperature range of 500-800°C indicated that the Ag might be an excellent intermetallic diffusion barrier. However, the effectiveness of a pure-Ag layer as an intermetallic diffusion barrier was limited by the non-uniformity of the electroless deposition morphology obtained from regular Ag plating baths.

◊ In an effort to improve the deposition morphology and to achieve uniform Ag layers, the conventional electroless plating bath was modified by using a concentrated Ag plating solution (61.2 mM). The Ag layer formed by the concentrated Ag plating bath was termed as the "pure-Ag barrier" layer and successfully utilized to deposit 3-5 μm thick Ag layers and for the synthesis of Pd/Ag layers with an Ag content as high as 30-40 wt%.

◊ Coupled with the long-term H_2 permeation data for several Pd/Ag membranes, the detailed cross-sectional SEI and EDX analyses led to the conclusion that the pure-Ag barrier layer was effective against intermetallic diffusion.

◊ Furthermore, an *in-situ* oxidation study indicated that the formation of a Cr-rich oxide layer for the Ni-rich porous sintered metal supports was possible at an oxidation temperature of 800°C, as evidenced by the weight gain, surface SEI micrographs and the XRD phase identification analyses.

◊ The combined use of pure-Ag barrier layer, $Al(OH)_3$ grading technique and the support oxidation temperature of 800°C for the synthesis of 11.6 μm thick Pd/Ag membrane (31.7 wt% Ag) provided a stable H_2 permeance of 34.9 m^3/ m^2-h-$atm^{0.5}$ and a good long-term chemical stability over a period of ~800 hours at 500°C. Indeed, the H_2/He selectivity of the membrane remained as high as ~500 after testing ~800 hours at 500°C.

◊ In an effort to mitigate leak formation during high temperature annealing of the Pd/Ag layers formed by the electroless plating and even enhance the hydrogen

permeance, preparation of nano-crystalline Pd/Ag alloy particles was investigated as an alternative synthesis route. Pd/Ag alloy nanoparticles with an average grain size of 4 nm and an Ag content of 25-30 wt% have been successfully synthesized at room temperature.

◊ Dip coating of the Pd/Ag alloy nanoparticles between electrolessly formed Pd and Ag layers led to a dense Pd/Ag (31 wt% Ag) membrane with a total thickness as thin as 4.6 μm and showed a hydrogen permeance of 32 m^3/m^2-h-$atm^{0.5}$ at 500°C. However, the selectivity of the Pd/Ag membrane was altered by the presence of Kirkendall voids and/or porosity as the result of the marked difference between the individual diffusion mobility of the dip-coated Pd/Ag alloy nanoparticles and that of Ag and Pd layers formed by the electroless plating. Since 500°C was above the Tamman temperature of Ag metal (T_{Tamman}=344°C) and well above the melting temperature of Pd/Ag alloy nanoparticles, the driving force for the formation of thermal vacancies have substantially increased.

◊ Detailed cross-sectional SEI and EDX analyses coupled with the HTXRD temperature-ramp annealing studies indicated that the interdiffusion between Ag and Pd metals during high temperature annealing resulted in various phenomena associated with the Kirkendall effect. These were the migration of macroscopic inclusions within the diffusion zone, the development of the diffusional porosity, the generation of internal stress and even deformation on a microscopic scale.

◊ *In-situ* time-resolved high-temperature X-ray diffraction (HTXRD) analysis has been successfully employed to conduct quantitative analyses of the Pd/Ag alloy phase nucleation and growth kinetics for the isothermal annealing at 500°C, 550°C and 600°C under H_2 atmosphere. The data analyses based on the Avrami and parabolic rate law models indicated that the formation of the Pd/Ag alloy phase was through one-dimensional diffusion controlled growth. The estimated apparent activation energies from the Avrami and the parabolic rate law were 236.5 and 185.6 kJ/mol, respectively, and in good agreement with the literature values (183-239.5 kJ/mol).

◊ The agreement between the HTXRD kinetics data, the cross-section SEI micrographs and the EDX line scans indicated that the deposition morphology had a significant effect on the Pd/Ag alloy phase growth kinetics. The difference in estimated activation energies might be related to the likelihood presence of heterogeneous nucleation sites, defects and imperfections at the original interface between Pd and Ag layers.

◊ Atomic absorption flame analysis was successfully utilized to investigate the effects of temperature, initial metal ion concentration, initial hydrazine concentration and bath agitation on the electroless plating rates of Pd and Ag metals.

◊ It was found that the electroless plating of both Pd and Ag were strongly affected by the external mass transfer in the absence of bath agitation. The external mass transfer limitations for both Pd and Ag deposition have been overcome at or above a stirring rate of 400 rpm, resulting in the maximum conversion of the plating reaction and dramatically shortened plating times with the added advantage of uniform deposition morphology as evidenced from the SEI micrographs.

◊ Finally, the use of bath agitation was further utilized for the synthesis of Pd and Pd/Ag membranes. The combined use of *in-situ* oxidation to form an intermetallic diffusion barrier, and $Al(OH)_3$ grading technique and the bath agitation at a rate of 400 rpm led to a composite Pd/Inconel membrane with a hydrogen selective dense Pd layer as thin as 4.7 μm. After a total testing period of 690 hours, a stable H_2 permeance and H_2/He selectivity at 400°C was 63 m^3/m^2-h-$atm^{0.5}$ and over 310, respectively.

13. Recommendations

In order to mitigate progressive leak growth in composite Pd and Pd/Ag membranes, further research should focus on:

- ◊ The intermediate annealing of the as-synthesized Pd and/or Ag layers at a temperature range of 500-600°C in an inert atmosphere such as He, N_2 or Ar, studied previously in our laboratory should be investigared further. This will allow minimizing the effect of low temperature processes (discussed in Section 11.2) on the leak formation. Indeed, the contribution of grain/cluster growth, in particular for Ag, and cluster sintering to the progressive leak growth can be reduced to a certain extent by the intermediate annealing of the as-synthesized Pd and/or Ag layers. In the case of Pd/Ag layers, the annealing in H_2 atmosphere above 550°C should be avoided in order to eliminate the Kirkendall effect.

- ◊ A permanent solution to progressive leak growth may require the use of un-conventional approaches such as the *in-situ* leak repair via CVD derived processes. The aerosol-assisted or direct liquid injection type CVD processes are commonly applied for the fabrication of micro-electronic deveices. For this purpose, acetylacetonato complexes of Pd and/or Ag may be admitted to a modified permeator cell at low temperatures under an inert atmosphere such as He, N_2 or Ar. The sublimation temperatures for such complexes vary in the range of 60-160°C. The volatile components formed during sublimation can be easily discharged by applying vacuum from either shell-side (retentate) or tube-side (permeate) of the permeator cell. Indeed, the decomposition temperatures for the

acetylacetonato complexes are in the range of 200-270°C. Similarly, the deposition of Pd and/or Ag can be directed to the defected surface sites by applying vacuum from the tube-side in the presence of an inert atmosphere. The current H_2 permation test systems are well-suited for both controlling the decomposition temperature and instantaneously monitoring and logging the effect of *in-situ* leak repair on membrane selectivity.

The HTXRD data used to study the isothermal nucleation and growth kinetics of the Pd/Ag alloy phase transformation can be further utilized:

◊ To estimate the Pd/Ag interdiffusion coefficient in the temperature range of 500-600°C. This would allow accurate determination of high temperature annealing conditions. The preliminary analysis of the solution of the Fick's 2^{nd} law of diffusion indicated that the most widely used mathematical solutions such as the thin-film solution and the semi-infinite and/or infinite slab solutions were not suited for the HTXRD data. Therefore, more sophisticated moving-boundary solutions may be necessary. For this purpose, the Stefan problem might be adopted to estimate Pd/Ag interdiffusion coefficients. The Stefan problem is particularly suited for moving boundary value problems that are usually applied for the phase transitions in materials.

The effect of the bath agitation on the deposition morphology and the H_2 permeance characteristics of composite Pd and Pd/Ag membranes should be further investigated

◊ By conducting detailed cross-sectional SEI and EDX analysis

◊ By conducting high temperature annealing experiments and microstructure characterization studies to elucidate the effect of uniform deposition morphology on the coherent and/or incoherent sintering of the of the Pd and/or Ag clusters.

◊ By modifying the plating setup for the synthesis of large scale composite Pd and Pd/Ag membranes with bath agitation

◊ By conducting long-term H_2 permeance testing of the composite Pd and Pd/Ag membranes prepared on 1"OD and 6" long porous sintered metal supports.

References

Ackerman, F. J. and Koskinas, G. J. "Permeation of hydrogen and deuterium through palladium-silver alloys." *Journal of Chemical and Engineering Data*, **17**(1) (1972) 51-55.

Adda, Y. and Philibert, J. (1966). La Diffusion dans les Solides. Paris, France, Press. Univ.

Adrover, A.;Giola, M.;Capobianco, L.;Tripodi, P. and Violante, V. "Steady-state diffusion profiles of hydrogen in tubular metallic membranes." *International Journal of Hydrogen Energy*, **28** (2003) 1279-1284.

Akis, B. C.;Engwall, E. E.;Mardilovich, P. I. and Ma, Y. H. "Effects of the in-situ formation of an intermetallic diffusion barrier layer on the properties of composite palladium membranes." *American Chemical Society, Preprints*, **48**(1) (2003) 337-338.

Anderson, W. and Mehl, R. "Recrystallization of Al in terms of the rate of nucleation and growth." *Trans. AIME*, **161** (1945) 140.

Arkharov, V. I. *Trudy Inst. Fiz. Metal, Ural Fillial*, **14** (1954) 16-25.

Arkharov, V. I. and Yunikov, B. A. "Diffusion of Silver into Iron in the Presence of Small Additions of Palladium." *Trudy Inst. Fiz. Metal. Akad. Nauk S.S.S.R., Ural Fillial*, **16** (1955) 62-68.

Avdjukhina, V. M.;Katsnelson, A. A. and Revkevich, G. P. "Structural changes and their kinetics in hydrogen-containing palladium systems." *Platinum Metals Review*, **46**(4) (2002) 169-176.

Averbach, B. L. and Cohen, M. "X-ray Determination of Retained Austenite by Integrated Intensities." *Metals Technology*, **February** (1948) 1-14.

Avrami, M. "Kinetics of Phase Change. I: General Theory." *J. Chem. Phys.*, **7** (1939) 1103-1112.

Avrami, M. "Kinetics of Phase Change. II: Transformation-Time Relations for Random Distribution of Nuclei." *J. Chem. Phys.*, **8** (1940) 212-224.

Avrami, M. "Kinetics of Phase Change. III: Granulation, Phase Change on Microstructures." *J. Chem. Phys.*, **9** (1941) 177-184.

Axelrod, S. D. and Makrides, A. C. "X-Ray Studies of Hydrogen-Silver-Palladium Electrodes." *Journal of Physical Chemistry*, **68**(8) (1964) 2154.

Ayturk, M. E.;Engwall, E. E. and Ma, Y. H. "In-situ Annealing Strategies for Alloying of Pd/Ag-Alloy-Porous Stainless Steel (PSS) Membranes used for H_2 Separation."*Proceedings of the 8th*

International Conference on Inorganic Membranes (ICIM8), (2004a) Cincinnati, OH, United States.

Ayturk, M. E.;Engwall, E. E. and Ma, Y. H. "Challenges in the Formation of Composite Pd-Ag-Alloy/Porous Stainless Steel (PSS) Membranes for High Temperature H_2 Separation."*Proceedings of the Proceedings International Hydrogen Energy Congress and Exhibition (IHEC 2005)*, (2005a) Istanbul, Turkey.

Ayturk, M. E.;Engwall, E. E. and Ma, Y. H. "XRD Phase Analysis on the Alloying of Binary Pd/PSS, Ag/PSS and Ternary Pd/Ag/PSS Systems."*Proceedings of the 2005 North American Membrane Society Annual Meeting (NAMS 2005)*, (2005b) Providence, Rhode Island, United States.

Ayturk, M. E.;Engwall, E. E. and Ma, Y. H. "Microstructure Analysis of the Intermetallic Diffusion Induced Alloy Phases in Composite Pd/Ag/Porous Stainless Steel (PSS) Membranes." *Ind. Eng. Chem. Res.*, **In Press, 46**(12) (2007) xxx.

Ayturk, M. E.;Mardilovich, I. P.;Engwall, E. E. and Ma, Y. H. "Microstructure Analysis of Pd/Ag Alloy Membranes Supported on Porous Stainless Steel."*Proceedings of the AIChE Annual Meeting*, (2004b) Austin, TX.

Ayturk, M. E.;Mardilovich, I. P.;Engwall, E. E. and Ma, Y. H. "Synthesis of composite Pd-porous stainless steel (PSS) membranes with a Pd/Ag intermetallic diffusion barrier." *Journal of Membrane Science*, **285**(1-2) (2006) 385.

Balovnev, Y. A. "Diffusion of hydrogen in palladium." *Russian Journal of Physical Chemistry*, **48**(3) (1974) 409-410.

Basile, A.;Chiappetta, G.;Tosti, S. and Violante, V. "Experimental and simulation of both Pd and Pd/Ag for a water gas shift membrane reactor." *Separation and Purification Technology*, **25**(1-3) (2001) 549.

Beaty, R. B. and Kerber, J. D. (1993). Concepts, Instrumentation and Techniques in Atomic Absorption Spectroscopy. Norwalk, CT, U.S.A.

Becker, R. *Ann. Phys.*, **32** (1938) 128.

Becker, R. *Proc. Phys. Soc.*, **52** (1940) 71.

Birnbaum, H. K. and West, C. A. "Diffusion of hydrogen in metals." *Ber. Bundesges. Physik. Chem.*, **76** (1972) 806-816.

Bonyuet, D.;Ochoa, J. and Gonzales, G. "Mechanical Alloying in the Immiscible Systems Ag-M (M=Fe, Co, Ni)." *J. Metastable & Nanocrystl. Mater.*, **20-21** (2004) 225-230.

Brand, J. A. and Goldschmidth, H. j. "B.S.A. Group Research Center Sheffield, GRC/G 1109." (1955).

Brandes, E. A. and Brook, G. B. (1998). Smithells Metals Reference Book (7th Edition), Elsevier.

Brenner, A. and Riddell, G. *J. Res. Nat. 8ur. Std.*, **37** (1946) 3; ibid., 39,385.

Breteau, P. *Bull. SOC. Chim.* (1911) 9.

Brodowsky, H. and Poeschel, E. *Z. phys. Chem. N.F*, **44** (1965) 143.

Brown, A. M. and Ashby, M. F. "Correlations for diffusion constant." *Acta Metallurgica*, **28** (1980) 1085.

Bruning, K. and Sieverts, A. *Z. Phys. Chem.*, **163A** (1933) 409.

Bryden, K. J. and Ying, J. Y. "Nanostructured palladium-iron membranes for hydrogen separation and membrane hydrogenation reactions." *Journal of Membrane Science*, **203** (2002) 29-42.

Bucur, R. V., Ersson, N. O., Tong, X. Q. "Solubility and diffusivity of hydrogen in palladium and Pd77Ag23 containing lattice defects." *Journal of Less Common Metals*, **172-174** (1991) 748-758.

Burke, J. (1965). The kinetics of phase transformations in metals. Oxford, Pergamon Press Ltd.

Cahn, J. W. *Acta Metall.*, **4** (1956) 449.

Carson, A. W. and Lewis, F. A. "Pressure-composition Isotherms for the Pd+Ag+H System." *Trans. Faraday Soc.*, **63**(6) (1967) 1453.

Chen, Y.;Atago, T. and Mohri, T. "First Principles Study for Ordering and Phase Separation in the Fe-Pd System." *J. Phys.: Condens. Matter.*, **14** (2002) 1903-1913.

Cheng, Y. S.;Pena, M. A.;Fierro, J. L.;Hui, D. C. W. and Yeung, K. L. "Performance of alumina, zeolite, palladium, Pd-Ag alloy membranes for hydrogen separation from Towngas mixture." *Journal of Membrane Science*, **204**(1-2) (2002) 329.

Cheng, Y. S. and Yeung, K. L. "Palladium-silver composite membranes by electroless plating technique." *Journal of Membrane Science*, **158**(1-2) (1999) 127.

Choi, S. Y.;Mamak, M.;Speakman, S.;Chopra, N. and Ozin, G. A. "Evolution of nanocrystallinity in periodic mesoporous anatase thin films." *Small*, **1**(2) (2005) 226-232.

Christian, J. W. (1965). The theory of transformations in metals and alloys; an advanced textbook in physical metallurgy, Pergamon Press.

Collins, J. P. and Way, J. D. "Preparation and characterization of a composite Palladium-ceramic membrane." *Ind. Eng. Chem. Res.*, **32** (1993) 3006-3013.

Crank, J. (1975). The Mathematics of Diffusion. Ely House-London, Oxford University Press.

Cristensen, A.;Ruban, A. V.;Stoltze, P.;Jacobsen, K.;Skriver, H. L. and Norskov, J. K. "Phase Diagrams for Surface Alloys." *Physical Review B*, **56**(10) (1997) 5822-5833.

Cullity, B. D. and Stock, S. R. (2001). Elements of x-ray diffraction. Upper Saddle River, NJ, Prentice Hall, Edition: 3rd ed.

Damle, C.;Kumar, A. and Sastry, M. "Synthesis of Ag/Pd nanoparticles and their low temperature alloying within thermally evaporated fatty acid films." *J. Phys. Chem. B*, **106** (2002) 297-302.

Davis, W. *USAEC Report KAPL-1227, U. S. Atomic Energy Commission* (1954).

Deville, H. S. C. *C. r. hebd. Seanc. Acad. Sci., Paris*, **59** (1864) 102.

Deville, H. S. C. and Troost, L. *C. r. hebd. Seanc. Acad. Sci., Paris*, **57** (1863) 965.

Edlund, D. J. and McCarthy, J. "The relationship between intermetallic diffusion and flux decline in composite-metal membranes: implications for achieving long membrane lifetime." *Journal of Membrane Science*, **107**(1-2) (1995) 147.

Elkina, I. B. and Meldon, J. H. "Hydrogen transport in palladium membranes." *Desalination*, **147** (2002) 445-448.

Engwall, E. E.;Mardilovich, I. P. and Ma, Y. H. "Transport resistance for oxide diffusion barriers on porous metal supports used in composite Pd and Pd-alloy membranes." *Fuel Chemistry Division Preprints*, **48**(1) (2003) 390-391.

Fahler, S.;Weisheit, M. and Krebs, H.-U. "*In-situ* Characterization of Laser Deposited Fe/Ag Multilayers by a Combination of Time-of-Flight, RHEED and Resistance Measurements."*Proceedings of the Mat. Res. Soc. Symp. Proc.*, (1998).

Farr, J. P. G. and Harris, I. R. (1973).

Flanagan, T. B.;Gross, G. and Clewley, J. D. "Absorption and diffusion of hydrogen in palladium/iron alloys."*Proceedings of the Hydrogen in metals: Proceedings of the 2nd international congress*, (1977) Paris, Oxford; New York; Pergamon Press.

Flanagan, T. B. and Lewis, F. A. *Trans. Faraday Soc.*, **55** (1959) 1400-1409.

Fogler, H. S. (1992). Elements of Chemical Reaction Engineering. NJ, Prentice Hall International Inc.

Fort, D.;Farr, J. P. G. and Harris, I. R. *Journal of less common metals*, **39**(2) (1975) 293.

Friel, J. J. (1998). X-Ray and Image Analysis in Electron Microscopy. Princeton, NJ, Princeton-Gamma Tech.

Frieske, H. and Wicke, E. "Magnetic susceptibility and equilibrium diagram of PdH_n." *Ber. Bunsenges. Physik. Chem.*, **77** (1973) 48-52.

Frost, R. L.;Kloprogge, J. T.;Russell, S. C. and Szetu, J. L. "Vibrational spectroscopy and dehydroxylation of aluminum (oxo)hydroxides: Gibbsite." *Applied Spectroscopy*, **53** (1999) 423-434.

Gao, H.;S. Lin, J. Y.;Li, Y. and Zhang, B. "Electroless plating synthesis, characterization and permeation properties of Pd-Cu membranes supported on ZrO2 modified porous stainless steel." *Journal of Membrane Science*, **265**(1-2) (2005) 142.

Gao, H. Y.;Lin, Y. S.;Li, Y. D. and Zhang, B. Q. "Chemical stability and its improvements of Palladium-based metallic membranes." *Ind. Eng. Chem. Res.*, **43** (2004) 6920.

Gielens, F. C.;Tong, H. D.;van Rijn, C. J. M.;Vorstman, M. A. G. and Keurentjes, J. T. F. "High-flux palladium-silver alloy membranes fabricated by microsystem technology." *Desalination*, **147**(1-3) (2002) 417.

Gillespie, L. J. and Galstaun, L. S. "The palladium-hydrogen equilibrium and new palladium hydrides." *Journal of the American Chemical Society*, **58** (1936) 2565-2573.

Goto, S.;Assabumrungrat, S.;Tagawa, T. and Prasertham, P. "The effect of direction of hydrogen permeation on the rate through a composite palladium membrane." *J. Membrane Sci.*, **175** (2000) 19-24.

Graham, T. *Phil. Trans. R. Soc.*, **156** (1866) 415.

Graham, T. *Proc. R. Soc.*, **17** (1869a) 212.

Graham, T. *Proc. R. Soc.*, **17** (1869b) 500.

Gryaznov, V. "Metal containing membranes for the production of ultrapure hydrogen and the recovery of hydrogen isotopes." *Separation and Purification Methods*, **29**(2) (2000).

Gryaznov, V. M.;Serebyannikova, O. S. and Serov, Y. M. " Preparation and catalysis over palladium composite membranes." *Applied Catalysis A: General*, **96** (1993) 15-23.

Guazzone, F. (2005). Engineering of substrate surface for the synthesis of ultra-thin Pd and Pd-Cu membranes for H_2 separation. Chemical Engineering. Worcester, Worcester Polytechnic Institute. **PhD**.

Guazzone, F.;Ayturk, M. E. and Ma, Y. H. "Effect of intermetallic diffusion barrier on the stability of composite Pd/PSS membranes at high temperatures."*Proceedings of the 21st Annual International Pittsburgh Coal Conference*, (2004) Osaka, Japan.

Hasler, P. and Allmendinger, T. "Electrodeposition of thin Pd-Ag films." *Surface and Coatings Technology*, **58** (1993) 179-183.

Hermann, C.;Quicker, P. and Dittmeyer, R. "Mathematical simulation of catalytic dehydrogenation of ethylbenzene to styrene in a composite palladium membrane reactor." *J. Membrane Sci.*, **136** (1997) 161-172.

Hoang, H. T.;Tong, H. D.;Gielens, F. C.;Jansen, H. V. and Elwenspoek, M. C. "Fabrication and characterization of dual sputtered Pd-Cu alloy films for hydrogen separation membranes." *Materials Letters*, **58**(3-4) (2004) 525.

Hoffmann, R. E. and Turnbull, D. J. *J. Appl. Phys.*, **22** (1951) 634.

Höglund, L. and Agren, J. *J. Acta Mater.*, **49** (2001) 311.

Holleck, G. L. "Diffusion and solubility of hydrogen in palladium and palladium-silver alloys." *The journal of Physical Chemistry*, **74**(3) (1970) 503-511.

Hou, K. and Hughes, R. "The effect of external mass transfer, competitive adsorption and coking on hydrogen permeation through thin Pd/Ag membranes." *J. Membrane Sci.*, **206** (2002) 119-130.

Hou, K. and Hughes, R. "Preparation of thin and highly stable Pd/Ag composite membranes and simulative analysis of transfer resistance for hydrogen separation." *J. Membrane Sci.*, **214** (2003) 43-55.

Hou, S.;Jiang, K.;Li, W.;Xu, H. and Yuan, L. "A metal palladium composite membrane or alloy composite membrane and their preparation methods." **WO 2005/065806 A1** (2005).

Howard, B. H.;Killmeyer, R.;Rothenberger, K. S.;Ciocco, M. V.;Morreale, B. D.;Enick, R. M. and Bustamante, F. "The hydrogen permeability of palladium-copper alloys at elevated temperatures and pressures."*Proceedings of the MRS*, (2002).

Howard, B. H.;Killmeyer, R. P.;Rothenberger, K. S.;Cugini, A. V.;Morreale, B. D.;Enick, R. M. and Bustamante, F. "Hydrogen permeance of palladium-copper alloy membranes over a wide range of temperatures and pressures." *Journal of Membrane Science*, **241**(2) (2004) 207.

Huang, C.-Y.;Chiang, H.-J.;Huang, J.-C. and Sheen, S.-R. "Synthesis of nanocrystalline Ag-Pd alloys by chemical reduction method." *NanoStructured Materials*, **10**(8) (1998) 1393-1400.

Huang, T.-C.;Wei, M.-C. and Chen, H.-I. "Preparation of hydrogen-permselective palladium-silver alloy composite membranes by electroless co-deposition." *Separation and Purification Technology*, **32** (2003) 239-245.

Hunter, J. B. "A new hydrogen purification process." *Plat. Met. Rev.*, **4** (1960) 130-131.

Hurlbert, R. C. and Konecny, J. O. "Diffusion of hydrogen through palladium." *J. Chem. Phys.*, **34**(2) (1961) 655-658.

Itoh, N.;Wu, T. and Haraya, K. "Two-and three-dimensional analysis of diffusion through a dense membrane supported on a porous material." *J. Membrane Sci.*, **99** (1995) 175-183.

IUPAC. "IUPAC Compendium of Chemical Terminology, Electronic version, http://goldbook.iupac.org/." (2005).

JADE4.0 A program for powder diffraction data analysis. Livermore, CA, USA, Materials Data Inc.

Jarosch, K. and de Lasa, H. I. "Novel Riser Simulator for Methane Reforming using High Temperature Membranes." *Chemical Engineering Science*, **54** (1999) 1455-1460.

Jayaraman, V. and Lin, Y. S. "Synthesis and hydrogen permeation properties of ultrathin palladium-silver alloy membranes." *Journal of Membrane Science*, **104**(3) (1995) 251.

Jeema, N.;Grandjean, B. P. A. and Kaliaguine., S. "Diffusion coefficient of hydrogen in a Pd-Ag membrane: effect of hydrogen solubility." *The Canadian Journal of Chemical Engineering*, **73** (1995) 405-410.

Jeema, N.;Shu, J.;Kaliaguine, S. and Grandjean, B. P. A. "Thin Palladium Film Formation on Shot Peening Modified Porous Stainless Steel Substrates." *Ind. Eng. Chem. Res.*, **35**(3) (1996) 973-977.

Jemaa, N.;Shu, J.;Kaliaguine, S. and Grandjean, B. P. A. "Thin Palladium Film Formation on Shot Peening Modified Porous Stainless Steel Substrates." *Ind. Eng. Chem. Res.*, **35**(3) (1996) 973-977.

Johnson, W. and Mehl, R. "Reaction kinetics in processes of nucleation and growth." *Trans. AIME*, **135** (1939) 416-458.

Jun, C.-S. and Lee, K.-H. "Palladium and palladium alloy composite membranes prepared by metal-organic chemical vapor deposition method (cold-wall)." *Journal of Membrane Science*, **176**(1) (2000) 121.

Kajiwara, M.;Uemiya, S.;Kojima, T. and Kikuchi, E. "Rhodium- and iridium-dispersed porous alumina membranes and their hydrogen permeation properties." *Catalysis Today*, **56**(1-3) (2000) 83.

Kamakoti, P.;Morreale, B. D.;Ciocco, M. V.;Howard, B. H.;Killmeyer, R. P.;Cugini, A. V. and Sholl, D. S. "Prediction of Hydrogen Flux Through Sulfur-Tolerant Binary Alloy Membranes." *Science*, **307**(5709) (2005) 569.

Kamakoti, P. and Sholl, D. S. "A comparison of hydrogen diffusivities in Pd and CuPd alloys using density functional theory." *Journal of Membrane Science*, **225**(1-2) (2003) 145.

Karakaya, I. and Thompson, W. T. "The Pd-Ag System." *Bull. Alloy Phase Diagrams*, **9**(3) (1988) 237-243.

Karpova, R. A. and Tverdovskii, I. P. *J. Scient. Instrum.*, **33** (1959) 615.

Ke, X. and Kramer, G. J. "Absorption and diffusion of hydrogen in palladium-silver alloys by density functional theory." *Physical Review B*, **66** (2002) 184304.

Keuler, J. N. and Lorenzen, L. "Developing a heating procedure to optimize hydrogen permeance through Pd-Ag membranes of thickness less than 2.2 μm." *Journal of Membrane Science*, **195**(2) (2002) 203.

Keuler, J. N.;Lorenzen, L.;Sanderson, R. D.;Prozesky, V. and Pryzbylowicz, W. J. "Characterization of electroless plated palladium-silver alloy membranes." *Thin Solid Films*, **347** (1999a) 91-98.

Keuler, J. N.;Lorenzen, L.;Sanderson, R. D.;Prozesky, V. and Pryzbylowicz, W. J. "Characterizing palladium-silver and palladium-nickel alloy membranes using SEM, XRD and PIXE." *Nuclear Instruments and Methods in Physics Research B*, **158** (1999b) 678-682.

Keurentjes, J. T. F.;Gielens, F. C.;Tong, H. D.;vanRijn, C. J. M. and Vorstman, M. A. G. "High-Flux Palladium Membranes Based on Microsystem Technology." *Ind. Eng. Chem. Res.*, **43**(16) (2004) 4768-4772.

Kikuchi, E. "Palladium/ceramic membranes for selective hydrogen permeation and their application to membrane reactor." *Catalysis Today*, **25**(3-4) (1995) 333.

Kikuchi, E. "Membrane reactor application to hydrogen production." *Catalysis Today*, **56**(1-3) (2000) 97.

Kikuchi, E.;Nemoto, Y.;Kajiwara, M.;Uemiya, S. and Kojima, T. "Steam reforming of methane in membrane reactors: comparison of electroless-plating and CVD membranes and catalyst packing modes." *Catalysis Today*, **56**(1-3) (2000) 75.

Kikuchi, E. and Uemiya, S. "Preparation of supported thin palladium-silver alloy membranes and their characteristics for hydrogen separation." *Gas Separation & Purification*, **5**(4) (1991) 261.

Kim, S.;Kim, K.;Kacynski, R. M.;Acher, R. D.;Yoon, S.;Anderson, T. J.;Payzant, E. A. and Li, S. S. "Reaction kinetics of $CuInSe_2$ thin films grown from bilayer InSe/CuSe precursors." *J. Vac. Sci. Technol. A*, **23**(2) (2005) 310-315.

King, H. W.;Payzant, E. A. and Caughlin, T. A. "Temperature discrepancies in high temperature diffractometery." *Advances in X-Ray Analysis*, **40** (1997-1998) 679.

Kirk-Othmer (2004). Kirk-Othmer Encyclopedia of Chemical Technology, Wiley-Interscience.

Kirkendall, E.;Thomassen, L. and Upthegrove, C. "Rates of Diffusion of Copper and Zinc in Alpha Brass." *Trans. AIME*, **133** (1939) 186-203.

Kirkendall, E. O. "Diffusion of Zinc in Alpha Brass." *Trans. AIME*, **147** (1942) 104-110.

Kleppa, O. J. "The Solid State: Diffusion in Metals and Alloys." *Annu. Rev. Phys. Chem.*, **6** (1955) 119-140.

Knapton, A. G. "Palladium alloys for hydrogen diffusion membranes-A review of high permeability materials." *Plat. Met. Rev.*, **21** (1977) 44-50.

Koffler, S. A.;Hudson, J. B. and Ansell, G. S. "Hydrogen permeation through alpha-palladium." *Transactions of the Metallurgical Society of AIME*, **245** (1969) 1735-1740.

Kolmogorov, A. "A statistical theory for the recrystallization of metals." *Akad. nauk. SSSR, Izv., Ser. Matem.*, **1** (1937) 355.

Kulprathipanja, A.;Alptekin, G. O.;Falconer, J. L. and Way, J. D. "Pd and Pd-Cu membranes: inhibition of H2 permeation by H2S." *Journal of Membrane Science*, **254**(1-2) (2005) 49.

Kurokawa, H.;Nakayama, T.;Kobayashi, Y.;Suzuki, K.;Takahasyi, M.;Takami, S.;Kubo, M.;Itoh, N.;Selvam, P. and Miyamoto, A. "Monte Carlo simulation of hydrogen absorption in palladium and palladium-silver alloys." *Catalysis Today*, **82** (2003) 233-240.

Latyshev, V. V. and Bystritskiy, V. M. "Interaction of hydrogen isotopes and diffusion membranes made from palladium alloys." *Phys. Met. Metall.*, **71**(6) (1991) 1-20.

Latyshev, V. V. and Gur'yanov, V. G. "The interaction of hydrogen with palladium-based alloy membranes." *Russian Journal of Physical Chemistry*, **62**(2) (1988) 220-224.

Latyshev, V. V. and Gur'yanov, V. G. "The interaction of hydrogen with palladium-based alloy membranes." *Russian Journal of Physical Chemistry*, **62**(2) (1998) 220-224.

Latyshev, V. V.;Gur'yanov, V. G.;Asliddinova, M. Y.;Cholovyan, I. I. and Mironova, G. I. "Hydrogen-stimulated impurity diffusion through palladium-alloy membranes." *Sov. Phys. Tech. Phys.*, **36**(9) (1991) 1058-1059.

Lee, D.-W.;Lee, Y.-G.;Nam, S.-E.;Ihm, S.-K. and Lee, K.-H. "Study on the variation of morphology and separation behavior of the stainless steel supported membranes at high temperature." *Journal of Membrane Science*, **220**(1-2) (2003) 137.

Lewis, F. A. (1967). The palladium hydrogen system, London, New York, Academic Press.

Li, A.;Liang, W. and Hughes, R. "Repair of Pd/α-Al_2O_3 composite membrane containing defects." *Separation and Purification Technology*, **15** (1999) 113-119.

Li, A.;Liang, W. and Hughes, R. "Fabrication of dense palladium composite membranes for hydrogen separation." *Catalysis today*, **56** (2000) 45-51.

Li, A., Liang, Weiqiang, Hughes, Ronald. "Characterization and permeation of palladium/stainless steel composite membranes." *J. Membrane Sci.*, **149** (1998) 259-268.

Li, Y. and Cheng, Y.-T. "Hydrogen diffusion and solubility in palladium thin films." *International Journal of Hydrogen Energy*, **21**(4) (1996) 281-291.

Li, Z. Y.;Maeda, H.;Kusakabe, K.;Morooka, S.;Anzai, H. and Akiyama, S. "Preparation of palladium-silver membranes for hydrogen separation by the spray pyrolysis method." *Journal of Membrane Science*, **78** (1993) 247-254.

Lin, Y.-M.;Liu, S.-L.;Chuang, C.-H. and Chu, Y.-T. "Effect of incipient removal of hydrogen through palladium membrane on the conversion of methane steam reforming experimental and modeling." *Catalysis Today*, **82** (2003) 127-139.

Lin, Y.-M. and Rei, M.-H. "Study on the hydrogen production from methanol steam reforming in supported palladium membrane reactor." *Catalysis Today*, **67**(1-3) (2001) 77.

Lind, C.;Angus, P.;Wilkinson, P.;Rawn, J. and Payzant, E. A. "Kinetics of the cubic trigonal transformation in $ZrMo_2O_8$ and their dependence on precursor chemistry." *J. Mater. Chem.*, **12** (2002) 990-994.

Ma, Y. H.;Akis, B. C.;Ayturk, M. E.;Guazzone, F.;Engwall, E. E. and Mardilovich, I. P. "Characterization of Intermetallic Diffusion Barrier and Alloy Formation for Pd/Cu and Pd/Ag Porous Stainless Steel Composite Membranes." *Ind. Eng. Chem. Res.*, **43**(12) (2004a) 2936-2945.

Ma, Y. H.;Engwall, E. E. and Mardilovich, I. P. "Composite palladium and palladium-alloy membranes for high temperature hydrogen separations." *Fuel Chemistry Division Preprints*, **48**(1) (2003) 333-334.

Ma, Y. H. and Guazzone, F. "Composite gas separation modules having a layer of particles with a uniform binder metal distribution." **United States Patent Application 20060016332** (2006).

Ma, Y. H.;Mardilovich, I. P. and Engwall, E. E. "Composite Gas Modules Having Intermediate Porous Metal Layers." **US Provisional Patent Application US2004.0237779 A1** (2004b).

Ma, Y. H.;Mardilovich, I. P. and Engwall, E. E. "Composite Gas Modules Having Intermediate Porous Metal Layers." **US Patent 7,175,694** (2007).

Ma, Y. H.;Mardilovich, I. P. and Mardilovich, P. P. "Effects of porosity and pore size distribution of the porous stainless steel on the thickness and hydrogen flux of palladium membranes." *Journal of American Chemical Society*, **46**(2) (2001) xxx.

Ma, Y. H.;Mardilovich, P. P. and She, Y. "Hydrogen gas-extraction module and method of fabrication." **US Patent 6,152,987** (2000).

Magee, C. L. *Metall. Trans.*, **2** (1971) 2419.

Makrides, A. C. "Absorption of hydrogen by silver-palladium alloys." *The Journal of Physical Chemistry*, **68**(8) (1964) 2169-2169.

Mallory, G. O. and Hajdu, J. B. (1990). Electroless Plating-Fundamentals and Applications, William Andrew Publishing/Noyes.

Mardilovich, I. P.;Engwall, E. and Ma, Y. H. "Dependence of hydrogen flux on the pore size and plating surface topology of asymmetric Pd-porous stainless steel membranes." *Desalination*, **144**(1-3) (2002) 85.

Mardilovich, I. P.;Engwall, E. E. and Ma, Y. H. "Thermally Stable Composite Pd Membranes Having Intermediate Porous Metal Intermetallic Diffusion Barrier Layers Formed By Bi-Metal Multi-Layer Deposition."*Proceedings of the 9th International Conference on Inorganic Membranes (ICIM9)*, (2006) Lillehammer, Norway.

Mardilovich, P. P.;She, Y.;Ma, Y. H. and Rei, M.-H. "Defect-Free Palladium Membranes on Porous Stainless-Steel Support." *AIChE Journal*, **44**(2) (1998a) 310.

Mardilovich, P. P.;She, Y.;Ma, Y. H. and Rei, M. H. "Stability of Hydrogen Flux Through Pd/Porous Stainless Steel Composite Membranes."*Proceedings of the 5th International Conference on Inorganic Membranes (ICIM5)*, (1998b) Nagoya-Japan.

McCool, B.;Xomeritakis, G. and Lin, Y. S. "Composition control and hydrogen permeation characteristics of sputter deposited palladium-silver membranes." *Journal of Membrane Science*, **161**(1-2) (1999) 67.

McKinley, D. L. **U.S patent 3,350,845** (1967).

McKinley, D. L. **U.S patent 3,439,474** (1969).

Morreale, B. D.;Ciocco, M. V.;Enick, R. M.;Morsi, B. I.;Howard, B. H.;Cugini, A. V. and Rothenberger, K. S. "The permeability of hydrogen in bulk palladium at elevated temperatures and pressures." *Journal of Membrane Science*, **212**(1-2) (2003) 87.

Morreale, B. D.;Ciocco, M. V.;Howard, B. H.;Killmeyer, R. P.;Cugini, A. V. and Enick, R. M. "Effect of hydrogen-sulfide on the hydrogen permeance of palladium-copper alloys at elevated temperatures." *Journal of Membrane Science*, **241**(2) (2004) 219.

Moss, T. S.;Peachey, N. M.;Snow, R. C. and Dye, R. C. "Multilayer metal membranes for hydrogen separation." *International Journal of Hydrogen Energy*, **23**(2) (1998) 99-106.

Nachtrieb, N. H.;Petit, J. and Wehrenberg, J. "Self-Diffusion of Ag in Silver-Palladium Alloys." *J. Chem. Phys.*, **26** (1957) 106.

Nam, S.-E. and Lee, K.-H. "A study on the palladium/nickel composite membrane by vacuum electrodeposition." *Journal of Membrane Science*, **170**(1) (2000) 91.

Nam, S.-E. and Lee, K.-H. "Hydrogen separation by Pd alloy composite membranes: introduction of diffusion barrier." *Journal of Membrane Science*, **192**(1-2) (2001) 177.

Nam, S.-E.;Lee, S.-H. and Lee, K.-H. "Preparation of a palladium alloy composite membrane supported in a porous stainless steel by vacuum electrodeposition." *Journal of Membrane Science*, **153**(2) (1999) 163.

Nam, S. E. and Lee, K. H. "Preparation and Characterization of Palladium Alloy Composite Membranes with a Diffusion Barrier for Hydrogen Separation." *Ind. Eng. Chem. Res.*, **44**(1) (2005) 100-105.

Nash, A. (1990). The Pd-Ni System. Materials Park, OH, ASM International.

Neumann, G. and Tolle, V. *Phil. Mag. A*, **54** (1986) 619.

Norberg, R. E. *Phys. Rev.*, **86** (1952) 745.

Norris, A. C. (1981). Computational Chemistry-An Introduction to Numerical Solution. New York, Wiley.

O'Brien, J.;Hughes, R. and Hisek, J. "Pd/Ag membranes on porous alumina substrates by unbalanced magnetron sputtering." *Surface and Coatings Technology*, **142-144** (2001) 253-259.

Okamoto, H. and Masalski, T. B. (1990). Binary Alloy Phase Diagrams, ASM International.

Ozaki, T.;Zhang, Y.;Komaki, M. and Nishimura, C. "Preparation of palladium-coated V and V-15Ni membranes for hydrogen purification by electroless plating technique." *International Journal of Hydrogen Energy*, **28** (2003) 297-302.

Pan, X. L.;Stroh, N.;Brunner, H.;Xiong, G. X. and Sheng, S. S. "Pd/ceramic hollow fibers for H2 separation." *Separation and Purification Technology*, **32** (2003) 265-270.

Peachey, N. M.;Snow, R. C. and Dye, R. C. "Composite Pd/Ta metal membranes for hydrogen separation." *Journal of Membrane Science*, **111**(1) (1996) 123.

Perry, R. H. and Green, D. W. (1997). Perry's Chemical Engineers' Handbook, 7th Edition, McGraw-Hill.

Peterson, N. L. *Phys. Rev.*, **132** (1963) 2471.

Peterson, N. L. *Phys. Rev.*, **136** (1964) 568.

Pluym, T. C.;Kodas, T. T.;Wang, L.-M. and Glicksman, H. D. "Silver-Palladium alloy particle production by spray pyrolysis." *Journal of Materials Research*, **10**(1661) (1996).

Porter, D. A. and Easterling, K. E. (1981). Phase transformations in metals and alloys, Van Nostrand Reinhold Company Ltd.

Porter, D. A. and Easterling, K. E. (1992). Phase Transformations in Metals and Alloys, CRC Press.

Prabnu, A. K.;Liu, A.;Lovell, L. G. and Oyama, S. T. "Modeling of methane steam reforming reaction in hydrogen selective membrane reactors." *J. Membrane Sci.*, **177** (2000) 83-95.

Rhoda, R. N. "Palladium plating by chemical reduction." (1959).

Roa, F.;Block, M. J. and Way, J. D. "The influence of alloy composition on the H2 flux of composite Pd-Cu membranes." *Desalination*, **147**(1-3) (2002) 411.

Roa, F. and Way, J. D. "Alloy composition effect on the n-value for H_2-selective membranes." *Fuel Chemistry Division Preprints*, **48**(1) (2003a) 335-336.

Roa, F. and Way, J. D. "Influence of alloy composition and membrane fabrication on the pressure dependence of the hydrogen flux of palladium-copper membranes." *Ind. Eng. Chem. Res.*, **42** (2003b) 5827-5835.

Roa, F. and Way, J. D. "The effect of air exposure on palladium-copper composite membranes." *Applied Surface Science*, **240**(1-4) (2005) 85.

Roa, F.;Way, J. D.;McCormick, R. L. and Paglieri, S. N. "Preparation and characterization of Pd-Cu composite membranes for hydrogen separation." *Chemical Engineering Journal*, **93**(1) (2003) 11-22.

Rodina, A. A.;Gurevich, M. A. and Doronicheva, N. I. "The interaction of hydrogen with certain palladium-gold and palladium-silver-gold alloys." *Russ. J. Phys. Chem.*, **45** (1971) 621-623.

Rothenberger, K. S.;Cugini, A. V.;Howard, B. H.;Killmeyer, R. P.;Ciocco, M. V.;Morreale, B. D.;Enick, R. M.;Bustamante, F.;Mardilovich, I. P. and Ma, Y. H. "High pressure hydrogen permeance of porous stainless steel coated with a thin palladium film via electroless plating." *Journal of Membrane Science*, **244**(1-2) (2004) 55.

Rothenberger, K. S.;Howard, B. H.;Killmeyer, R. P.;Cugini, A. V.;Enick, R. M.;Bustamante, F.;Ciocco, M. V.;Morreale, B. D. and Buxbaum, R. E. "Evaluation of tantalum-based materials for hydrogen separation at elevated temperatures and pressures." *Journal of Membrane Science*, **218**(1-2) (2003) 19.

Roux, F. A. (1916).

Rowland, R. L. and Nachtrieb, N. H. "Self-Diffusion if Palladium in Silver-Palladium Alloys." *J. Phys. Chem.*, **67** (1963) 2817.

Rubow, K. L. and Stange, L. "Sintered porous metal filtration systems for petroleum refining applications." *Advances in Filtration and Separation Technology*, **15** (2002) 488-499.

Saini, A. (2006). An investigation of the cause of leak formation in palladium composite membranes. Chemical Engineering. Worcester, Worcester Polytechnic Institute. **M.Sc.**

Sakamoto, Y.;Hirata, S. and Nishikawa, N. "Diffusivity and solubility of hydrogen in Pd-Ag and Pd-Au alloys." *Journal of Less Common Metals*, **88**(2) (1982) 387-395.

Sakamoto, Y.;Tanaka, H.;Sakamoto, F.;Lewis, F. A. and Tong, X. Q. "Self strain gradient induced diffusion of hydrogen in Pd-Ag alloy membranes." *International Journal of Hydrogen Energy*, **20**(1) (1995) 35.

Schober, H. R. and Stoneham, A. M. "Diffusion of hydrogen in transition metals." *Journal of Less Common Metals*, **172-174** (1991) 538-547.

Seizt, F. *Phys. Rev.*, **74** (1948) 1513.

Serra, E.;Kemali, M.;Perujo, A. and Ross, D. K. "Hydrogen and deuterium in Pd-25%Ag alloy: Permeation, diffusion, solubilization and surface reaction." *Metallurgical and Materials Transacctions A*, **29A**(3A) (1998) 1023-1028.

She, Y. (2000). Composite palladium membranes: synthesis, separation and reaction. Chemical Engineering. Worcester, Worcester Polytechnic Institute. **PhD**.

She, Y.;Han, J. and Ma, Y. H. "Palladium membrane reactor for the dehydrogenation of ethylbenzene to styrene." *Catalysis Today*, **67**(1-3) (2001) 43.

Shu, J.;A., G. B. P.;Van Neste, A. and Kaliaguine, S. "Catalytic palladium-based membrane reactors: a review." *The Canadian Journal of Chemical Engineering*, **69** (1991a) 1036-1060.

Shu, J.;Adnot, A.;Grandjean, B. P. A. and Kaliaguine, S. "Structurally stable composite Pd-Ag alloy membranes: Introduction of a diffusion barrier." *Thin Solid Films*, **286** (1996) 72-79.

Shu, J.;Bongondo, B. E. W.;Grandjean, B. P. A. and Kaliguine, S. "Morphological changes of Pd-Ag membranes upon hydrogen permeation." *Chapman & Hall*? (1997) 294-297.

Shu, J.;Grandjean, B. P. A.;Ghali, E. and Kaliaguine, S. "Simultaneous deposition of Pd and Ag on porous stainless steel by electroless plating." *Journal of Membrane Science*, **77**(2-3) (1993) 181.

Shu, J.;Grandjean, B. P. A. and Kaliguine, S. "Methane steam reforming in asymmetric Pd- and Pd-Ag/porous SS membrane reactors." *Applied Catalysis A: General*, **119** (1994) 305-325.

Shu, J.;Grandjean, B. P. A. and Kaliguine, S. "Asymmetric Pd-Ag/stainless steel catalytic membranes for methane steam reforming." *Catalysis Today*, **25** (1995) 327-332.

Shu, J.;Grandjean, B. P. A.;Van Neste, A. and Kaliaguine, S. "Catalytic palladium-based membrane reactors; a review." *The canadian journal of chemical engineering*, **69** (1991b) 1036-1060.

Sieverts, A.;Jurisch, E. and Metz, A. *Z. anorg. allg. Chem.*, **92** (1915) 329.

Silvert, P. Y.;Vijayakrishnan, V.;Vibert, P.;Herrera-Urbina, R. and Elhsissen, K. T. "Synthesis and Characterization of Nanoscale Ag-Pd Alloy Particles." *NanoStructured Materials*, **7**(6) (1996) 611-618.

Singleton, M. (1990). The Ag-Ni System. Materials Park, OH, ASM International.

Smigelskas, A. D. and Kirkendall, E. O. "Zinc Diffusion in Alpha Brass." *Trans. AIME*, **171** (1947) 130-142.

Smoluchowski, R. *Phys. Rev.*, **87** (1952) 482.

So, J.-H.;Yang, S.-M. and Bin Park, S. "Preparation of silica-alumina composite membranes for hydrogen separation by multi-step pore modifications." *Journal of Membrane Science*, **147**(2) (1998) 147.

Sonwane, C. G.;Wilcox, J. and H., M. Y. "Achieving optimum hydrogen permeability in PdAg and PdAu alloys." *J. Chem. Phys.*, **125**(18) (2006a).

Sonwane, C. G.;Wilcox, J. and H., M. Y. "Solubility of Hydrogen in PdAg and PdAu Binary Alloys Using Density Functional Theory." *Journal of Physical Chemistry B*, **110**(48) (2006b) 24549-24558.

Souleimanova, R. S.;Mukasyan, A. S. and Varma, A. "Study of structure formation during electroless plating of thin metal-composite membranes." *Chemical Engineering Science*, **54** (1999) 3369-3377.

Souleimanova, R. S.;Mukasyan, A. S. and Varma, A. "Effects of osmosis on microstructure of Pd-composite membranes synthesized by electroless plating technique." *Journal of Membrane Science*, **166**(2) (2000) 249.

Souleimanova, R. S.;S., M. A. and Varma, A. "Pd-composite membranes prepared by electroless plating and osmosis: synthesis, characterization and properties." *Separation and Purification Technology*, **25**(1-3) (2001) 79-86.

Su, C.;Jin, T.;Kuraoka, K.;Matsumura, Y. and Yazawa, T. "Thin Palladium Film Supported on SiO_2-Modified Porous Stainless Steel for a High-Hydrogen-Flux Membrane." *Ind. Eng. Chem. Res.*, **44**(9) (2005) 3053-3058.

Subramanian, P. R. and Laughlin, D. E. "Cu-Pd (Copper-Palladium)." *Journal of Phase Equilibria*, **12**(2) (1991).

Swartzendruber, L. G. "The Ag-Fe System." *Bull. Alloy Phase Diagrams*, **5**(6) (1984) 560-564.

Thomann, A.-L.;Rozenbaum, J. P.;Brault, P.;Andreazza-Vignolle, C. and Andreazza, P. "Pd nanoclusters grown by plasma sputtering deposition on amorpous substrates." *Applied Surface Science*, **158** (2000) 172-183.

Thomas, S., Schäfer, R., Caro, J., Seidel-Morgenstern, A. "Investigation of mass transfer through inorganic membranes with several layers." *Catalysis Today*, **67** (2001) 205-216.

Toda, G. *J. Res. Inst. Catalysis Hokkaido Univ.*, **6** (1958) 13.

Tong, H. D.;Gielens, F. C.;Gardeniers, J. G. E.;Jansen, H. V.;vanRijn, C. J. M.;Elwenspoek, M. C. and Nijdam, W. "Microfabricated Palladium-Silver Alloy Membranes and Their Application in Hydrogen Separation." *Ind. Eng. Chem. Res.*, **43**(15) (2004a) 4182-4187.

Tong, J.;Kashima, Y.;Shirai, R.;Suda, H. and Matsumura, Y. "Thin Defect-Free Pd Membrane Deposited on Asymmetric Porous Stainless Steel Substrate." *Ind. Eng. Chem. Res.*, **44**(21) (2005a) 8025-8032.

Tong, J. and Matsumura, Y. "Thin Pd membrane prepared on macroporous stainless steel tube filter by an in-situ multi-dimensional plating mechanism." *Chem. Commun.* (2004) 2460-2461.

Tong, J. and Matsumura, Y. "Effect of catalytic activity on methane steam reforming in hydrogen-permeable membrane reactor." *Applied Catalysis A: General*, **286**(2) (2005) 226.

Tong, J.;Matsumura, Y.;Suda, H. and Haraya, K. "Experimental study of steam reforming of methane in a thin (6 μm) Pd-based membrane reactor." *Ind. Eng. Chem. Res.*, **44** (2005b) 1454-1465.

Tong, J.;Matsumura, Y.;Suda, H. and Haraya, K. "Thin and dense Pd/CeO2/MPSS composite membrane for hydrogen separation and steam reforming of methane." *Separation and Purification Technology*, **46**(1-2) (2005c) 1.

Tong, J.;Shirai, R.;Kashima, Y. and Matsumura, Y. "Preparation of a pinhole-free Pd-Ag membrane on a porous metal support for pure hydrogen separation." *Journal of Membrane Science*, **260**(1-2) (2005d) 84-89.

Tong, J.;Su, C.;Kuraoka, K.;Suda, H. and Matsumura, Y. "Preparation of thin Pd membrane on CeO2-modified porous metal by a combined method of electroless plating and chemical vapor deposition." *Journal of Membrane Science*, **269** (2006a) 101-108.

Tong, J.;Su, L.;Haraya, K. and Suda, H. "Thin and defect-free Pd-based composite membrane without any interlayer or substrate penetration by a combined organic and inorgani process." *Chem. Commun.* (2006b) 1142-1144.

Tong, J.;Suda, H.;Haraya, K. and Matsumura, Y. "A novel method for the preparation of thin dense Pd membrane on macroporous stainless steel tube filter." *Journal of Membrane Science*, **260**(1-2) (2005e) 10-18.

Tong, J.;Xu, H.;Wang, D. and Matsumura, Y. "Preparation of thin palladium membrane on porous stainless steel support modified with cerium hydroxide." *J. Jpn. Petrol. Inst.*, **47**(1) (2004b) 64-65.

Tosti, S. "Supported and laminated Pd-based metallic membranes." *International Journal of Hydrogen Energy*, **28**(12) (2003) 1445.

Tosti, S.;Adrover, A.;Basile, A.;Camilli, V.;Chiappetta, G. and Violante, V. "Characterization of thin wall Pd-Ag rolled membranes." *International Journal of Hydrogen Energy*, **28**(1) (2003a) 105.

Tosti, S.;Basile, A.;Chiappetta, G.;Rizzello, C. and Violante, V. "Pd-Ag membrane reactors for water gas shift reaction." *Chemical Engineering Journal*, **93**(1) (2003b) 23.

Tosti, S.;Bettinali, L.;Castelli, S.;Sarto, F.;Scaglione, S. and Violante, V. "Sputtered, electroless, and rolled palladium-ceramic membranes." *Journal of Membrane Science*, **196**(2) (2002) 241.

Tosti, S.;Bettinali, L. and Violante, V. "Rolled thin Pd and Pd-Ag membranes for hydrogen separation and production." *International Journal of Hydrogen Energy*, **25**(4) (2000) 319.

Touloukian, Y. S.;Kriby, R. K.;Taylor, R. E. and Desai, P. D. "Thermal expansion: metallic elements and alloys." *Thermophysical Properties of Matter*, **12** (1977) 298.

Troost, L. and Hautefeuille, P. *Annls. Chim. Phys.*, **2**(5) (1874) 273.

Uemiya, S.;Kato, W.;Uyama, A.;Kajiwara, M.;Kojima, T. and Kikuchi, E. "Separation of hydrogen from gas mixtures using supported platinum-group metal membranes." *Separation and Purification Technology*, **22-23** (2001) 309.

Uemiya, S.;Matsuda, T. and Kikuchi, E. "Hydrogen permeable palladium-silver alloy membrane supported on porous ceramics." *Journal of Membrane Science*, **56**(3) (1991a) 315.

Uemiya, S.;Mishima, S.;Makino, Y.;Miyazaki, I.;Moritomi, H. and Nishimura, M. "Novel method for fabrication of supported palladium membranes for membrane reactor." *Fuel Chemistry Division Preprints*, **48**(1) (2003) 339-340.

Uemiya, S.;Sato, N.;Ando, H.;Kude, Y.;Matsuda, T. and Kikuchi, E. "Separation of hydrogen through palladium thin film supported on a porous glass tube." *Journal of Membrane Science*, **56**(3) (1991b) 303.

Van Dal, M. J. H.;Pleumeekers, M. C. L. P.;Kodentsov, A. A. and Van Loo, F. J. J. *Acta. Mater.*, **48** (2000) 385.

Völkl, J. and Alefeld, G. (1978). Diffusion of hydrogen in metals. Hydrogen in metals, Vol I. Vol 28 of Topics in applied physics.

Walker, P. (2001). www.hydrogennow.org.

Wang, D.;Tong, J.;Xu, H. and Matsumura, Y. "Preparation of palladium membrane over porous stainless steel tube modified with zirconium oxide." *Catalysis Today*, **93-95** (2004) 689.

Wang, S. and Johnston, C. T. "Assignment of the structural OH stretching bands of gibbsite." *American Mineralogist*, **85** (2000) 739-744.

Ward, T. L. and Dao, T. "Model of hydrogen permeation behavior in palladium membranes." *Journal of Membrane Science*, **153**(2) (1999) 211.

Wicke, E. and Nernst, G. H. "Phase diagram and thermodynamic behavior of the system Pd/H2 and Pd/D2 at normal temperatures: H/D separation effects." *Ber. Bundesges. Physik. Chem.*, **68** (1964) 224-235.

Wijmans, J. G. and Baker, R. W. "The solution-diffusion model: a review." *J. Membrane Sci.*, **107** (1995) 1-21.

Wurtz, A. *Ann. Chim. et Phys.*, **3** (1844) 11.

Yepes, D.;Cornaglia, L. M.;Irusta, S. and Lombardo, E. A. "Different oxides used as diffusion barriers in composite hydrogen permeable membranes." *Journal of Membrane Science*, **274**(1-2) (2006) 92.

Yeung, K. L.;Christiansen, S. C. and Varma, A. "Palladium composite membranes by electroless plating technique. Relationships between plating kinetics, film microstructure and membrane performance." *J. Membrane Sci.*, **159** (1999) 107-122.

Yeung, K. L.;Sebastian, J. M. and Varma, A. "Novel preparation of Pd/Vycor composite membranes." *Catalysis today*, **25** (1995) 231-236.

Zhao, H.-B.;Xiong, G.-X. and Baron, G. V. "Preparation and characterization of palladium-based composite membranes by electroless plating and magnetron sputtering." *Catalysis Today*, **56** (2000) 89-96.

Zhao, H.;Xiong, G.;Stroh, N. and Brunner, H. "Preparation and characterization of Pd-Ag alloy composite membrane with magnetron sputtering." *Science in China (Serie B)*, **42**(6) (1999) 581-588.

Zhao, H. B.;Pflanz, K.;Gu, J. H.;Li, A. W.;Stroh, N.;Brunner, H. and Xiong, G. X. "Preparation of palladium composite membranes by modified electroless plating procedure." *Journal of Membrane Science*, **142**(2) (1998) 147.

Zheng, W. and Wu, L. "Preparation and pore size shrinkage of palladium-ceramic composite membrane by electroless plating under hydrothermal conditions." *Materials Science and Engineering A*, **283**(1-2) (2000) 122.

Nomenclature

A .....Measured absorbance (abs)

A .....Pre-exponential or frequency factor

A_b .....Cross-sectional area of incident beam (m^2)

A_t .....Total plating area (cm^2)

b .....Path length in AA (m or Å)

c .....Analyte concentration in AA (mg/L or mmol/L)

C_i .....Time-dependent concentration of species *i* (mol/L or mmol/L)

C_{i_0} .....Initial concentration of species *i* (mol/L or mmol/L)

$C_{H,i}$ .....Concentration of H_2 at the high and low pressure sides of the membrane (mol/m^3)

$\pm \frac{dC_i}{dt}$ .....Rate of disappearance or the formation of the i^{th} species (positive for the products and negative for the reactants)

D_H .....Diffusivity of hydrogen in Pd or Pd/alloys (m^2/s)

e .....Charge on electron (Coulombs)

E_a .....Activation energy (J/mol or kJ/mol)

E_{ii} .....Interaction energy for each pair of interstitials

ΔE^0 .....Change in the electrochemical potential of the cell (V)

f.....Atomic scattering factor

$F_{(hkl)}$.....Structure factor for the reflection *hkl*

F .....The Faraday constant (96,500 Coulombs)

G_x .....Fraction of the total diffracted intensity contributed by a surface layer

ΔG .....The Gibbs free energy (J/mol or kJ/mol)

ΔH_s .....Enthalpy of absorption and/or solubility of hydrogen in Pd (J/mol or kJ/mol)

I_{hkl} .....Integrated intensity per unit length of diffraction line (J/m-s)

I_0 .....Intensity of incident beam (J/m^2-s)

J_{H_2} .....Hydrogen permeation flux (m^3/m^2-h or mol/m^2-s)

k_B .....The Boltzmann constant (1.38×10^{-23} J/mol)

k_i .....Rate constant for hydrogen absorption/desorption

K_S .....The Sieverts' constant or the equilibrium constant for the dissolution of atomic hydrogen ($atm^{0.5}$ or $Pa^{0.5}$)

$k(T)$ .....The temperature-dependent reaction rate constant

L .....The thickness of the membrane layer (m or μm)

L_s .....The wall thickness of the support (m or μm)

$L(T)$ .....The temperature-dependent lattice parameter of Ag (m or Å)

m .....The parabolic rate law exponent

m.....Mass of an electron ($9.1x10^{-31}$ kg)

Δm .....Weight gain (g or mg)

M .....Molecular weight (kg/kmol)

n .....Atomic H/Pd ratio or the Avrami exponent or the number of electrons transferred in the reaction

N_{i0} .....*Initial number of moles of species i at time t (moles)*

N_{i0} .....*Number of moles of species i at time t (moles)*

p.....Multiplicity factor

p_i .....Partial pressure of hydrogen (atm or Pa)

P .....Pressure of gas (atm or N/m^2)

$P_{H_2,i}$ .....Pressure of H_2 (atm or Pa)

$P_{ave.}$ .....Average pressure (atm or Pa)

ΔP .....Trans-membrane pressure (atm or Pa)

Q_H .....Hydrogen permeability (m^3-μm/m^2-h-$atm^{0.5}$ or kmol-m/m^2-s-$atm^{0.5}$)

Q_0 .....Pre-exponential or frequency factor for the hydrogen permeability

$\frac{Q_H}{L}$ .....Hydrogen permeance in (m^3/m^2-h-$atm^{0.5}$ or kmol/m^2-s-$atm^{0.5}$)

r .....Average pore radius (m or μm) or Radius of diffractometer circle (m)

R .....Universal gas constant (8.314 J/mol-K)

S_H .....Solubility of hydrogen in Pd or Pd/alloys (mol/m^3 or kmol/m^3)

T .....Temperature (°C or K)

V .....Unit volume (m^3)

x .....The X-ray penetration depth (μm)

X .....% Conversion (mols reacted per mols fed)

z_i .....Number of nearest neighbors for each of the interstitial hydrogen

Greek Symbols

α .....Fraction transformed for the product phase (i.e., Pd/Ag alloy)

$\alpha_K(T_i)$ .....The Knudsen flow coefficient at temperature T_i (m^3/m^2-h-atm)

$\alpha, \beta, \gamma...$ ...Reaction orders for the respective species

$\beta_v(T_i)$ .....The viscous (Poiseuille) flow coefficient at temperature T_i (m^3/m^2-h-atm^2)

ε .....Porosity

λ .....Mean free path of a molecule (m or Å) or the wavelength of incident beam (1.5406 Å for CuK_α radiation) or the wavelength dependent absorptivity coefficient

κ .....Hydrogen concentration constant (mol/m^3)

μ.....Linear absorption coefficient (m^{-1})

μ/ρ .....Mass absorption coefficient (cm^2/g)

μ_{mix} .....Linear absorption coefficient of the mixture (m^{-1})

$\mu(T_i)$ .....Viscosity of gas at temperature T_i (Pa.s)

Θ_i .....The Debye characteristic temperature of the substance *i* (K)

ρ .....Density (g/cm^3)

ν.....Volume of the unit cell (m^3 or $Å^3$)

$\bar{v}$ .....Mean molecular velocity (m/s)

τ .....Tortuosity

θ .....Fraction of sites occupied by hydrogen or surface coverage or the Bragg angle (radians)

Appendix A

A.1. Basic Principles of Atomic Absorption Spectroscopy

Atomic absorption spectroscopy (AA or AAS) is one of the most common instrumental methods for determining the concentration of a particular metal element within a sample. Instrumentation and applications for AAS greatly expanded after its development during the 1950s by a team of Australian chemists, lead by Alan Walsh, working at the CSIRO (Commonwealth Science and Industry Research Organisation) Division of Chemical Physics, in Melbourne Australia[38].

A typical instrumentation for the AAS consists of three major components: light source (2), atomizer (1) and light separation and detection units (3) as shown in Figure 3-7. Similarly, the operating conditions used for the *in-situ* measurement of electroless Pd and Ag kinetics via AAS (Perkin Elmer AA3100) were summarized in Table 3-6.

The light source is usually a hollow-cathode lamp of the element that is being measured. A cathode lamp is a stable light source, which is necessary to emit the sharp characteristic spectrum of the element to be determined. A different cathode lamp is needed for each element. Each time a lamp is changed, proper alignment is needed in order to get as much light as possible through the flame. Since AAS requires that the analyte atoms to be in the gas phase, ions or atoms in a sample must undergo desolvation and vaporization, which take place in atomizers. Flame AA uses a slot type burner to increase the path length, and therefore to increase the total absorbance. Sample solutions are usually aspirated with the gas flow into a nebulizing/mixing chamber to form small droplets before entering the flame. The nebulizer/mixing chamber thoroughly mixes acetylene (the fuel) and oxidant (air or nitrous oxide). The mixing of the fuel and the oxidant generates a negative pressure at the end of the plastic nebulizer tube. The uptake of the liquid sample into the nebulizer chamber by the help of the negative pressure is

[38] http://en.wikipedia.org/wiki/Atomic_absorption_spectroscopy

defined as the aspiration. A small glass impact bead and/or a fixed impeller inside the chamber generate a heterogeneous mixture of gases (fuel + oxidant) and suspended aerosol (finely dispersed sample). This mixture flows immediately into the burner head where it burns as a smooth, laminar flame evenly distributed along a narrow slot in the well-machined metal burner head. Liquid sample not flowing into the flame collects on the bottom of the nebulizer chamber and flows by gravity through a waste tube to a drainage vessel.

The light separation and detection in AA spectrometers is accomplished by the use of monochromators and detectors for UV and visible light. The main purpose of the monochromator is to isolate the specific absorption line emitted by the light source through spectral dispersion from background light due to interferences. Then the monochromator focuses the isolated spectrum upon a photomultiplier detector, whose function is to convert the light signal into an electrical signal.

Photomultiplier tubes (PMTS) are consisting of a photocathode and a series of dynodes in an evacuated glass enclosure, in which the photons that strike the photo-emissive cathode emit electrons due to the photoelectric effect. Instead of collecting these few electrons at an anode, the electrons are accelerated towards a series of additional electrodes called dynodes. These electrodes are each maintained at a more positive potential. Additional electrons are generated at each dynode. This cascading effect generates 105 to 107 electrons for each photon hitting the first cathode depending on the number of dynodes and the accelerating voltage. This amplified signal is finally collected at the anode where it can be measured. The processing of electrical signal is fulfilled by a signal amplifier. The signal could be displayed for readout, or further fed into a data station for printout by the requested format. Typically, the technique of atomic absorption spectroscopy (AAS) requires a liquid sample to be aspirated, aerosolized, and mixed with combustible gases, such as acetylene-air or acetylene-nitrous oxide. The mixture is ignited in a flame whose temperature ranges from 2100 to 2800°C. During combustion, atoms of the element of interest in the sample are reduced to free, unexcited ground state atoms, which absorb light at characteristic wavelengths. The ground state is defined as the state of least possible energy in a physical system, as of atoms or molecules. When

atoms or molecules absorb light, the incoming energy excites a quantized structure to a higher energy level (excited state), where the type of excitation depends on the wavelength of the light.

The characteristic wavelengths are element specific and accurate to 0.01-0.1nm. To provide element specific wavelengths, a light beam from a lamp whose cathode is made of the element being determined is passed through the flame. A device such as photon-multiplier can detect the amount of reduction of the light intensity due to absorption by the analyte, which can be directly related to the amount of the element in the sample.

A.2. Linear Calibration Curves

The relationship between the absorbance and the concentration of an absorbing species in a sample is accomplished by applying the Beer-Lambert Law as shown in Equation (A-1).

$$A = \lambda \times b \times c \qquad (A\text{-}1)$$

The Beer-Lambert law (or Beer's law) defined as the linear relationship between absorbance and concentration of an absorbing species, where A is the measured absorbance, λ is a wavelength-dependent absorptivity coefficient, b is the path length and c is the analyte concentration. An unknown concentration of an analyte can be determined by measuring the amount of light that a sample absorbs and applying Beer's law. The linearity of the Beer-Lambert law is limited by numerous chemical and instrumental factors including, deviations in absorptivity coefficients at high concentrations (>0.01M) due to electrostatic interactions between molecules in close proximity, scattering of light due to particulates in the sample, fluoresecence or phosphorescence of the sample, changes in refractive index at high analyte concentration, shifts in chemical equilibrium as a function of concentration, non-monochromatic radiation, stray light, disproportionate decomposition of molecules at high concentrations and un-absorbed radiation. If the absorptivity coefficient is not known, the unknown concentration of the analyte can be determined using a working curve (calibration curve) of absorbance versus concentration derived from standards. A typical calibration curves for Pd and Ag are given in Figure A-1.

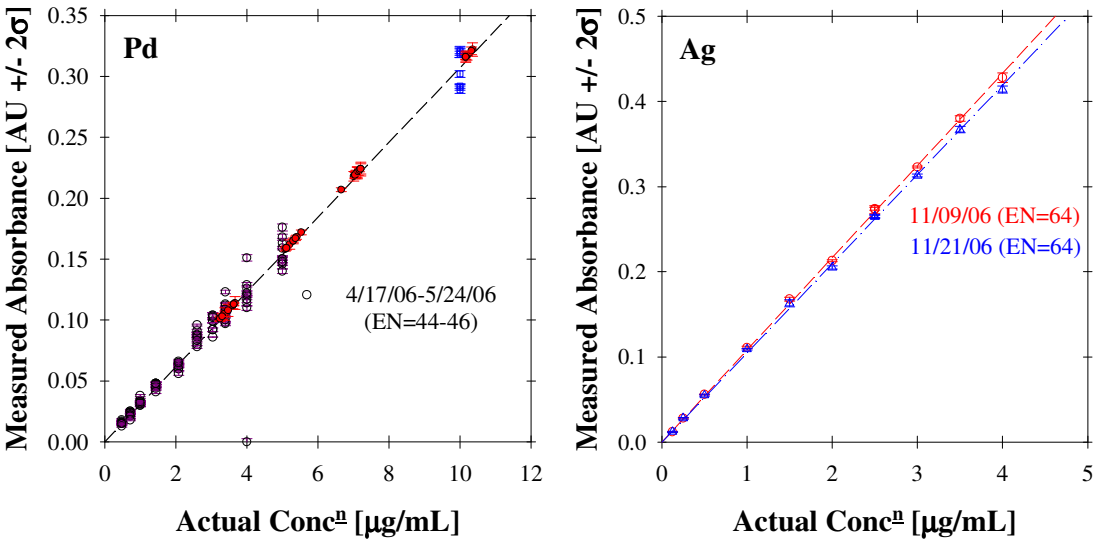

Figure A-1: Sample calibration curves for Pd and Ag

A.3. The Method of Standard Additions

Although the determination of the linear calibration curves is not trivial, the accuracy of the analysis may be limited by the presence of interferences in the samples matrix. The interferences in atomic absorption analysis fall into six categories: These categories were described by Beaty and Kerber (1993) and are:

1. Chemical interferences: If the energy of the flame is too low to decompose a thermally stable compound in the analyte. The energy of the Air-C_2H_2 flame (2125-2400°C) was high enough to decompose both Pd and Ag metals. There were no chemical interferences in the case of Pd and Ag solutions.

2. Ionization interferences: If the flame temperature has enough energy to cause the removal of an electron from the atom, thus, producing an ion (there were no ionization interferences in the case of Pd and Ag solutions).

3. Emission interferences: Low emission signal due to the presence of highly emissive elements (i.e., Ba). There were no emission interferences in the case of Pd and Ag solutions.

4. Spectral interferences: If there is an interfering element present at the same AA signal, which is usually seen when multi-element lamps are used. No possible spectral

interference was found for the Pd and Ag wavelengths 244.8 nm and 328.1 nm, respectively.

5. Background absorption: It can be avoided by switching to AA-BG mode or careful examination of the auto-zero offset value with the blank diluent solution between successive aspirations.

6. Matrix interferences: If the sample solution contains high concentration of dissolved salts or acids (i.e, plating solutions). Matrix interferences can be avoided by the use of the method of standard additions.

Among several different interferences described by Beaty and Kerber (1993), the matrix interference is of great importance especially if the sample solution contains high concentration of dissolved salts or acids, such as the plating solutions. The matrix interferences can be avoided by the use of the method of standard additions.

The method of standard additions is a useful technique, which makes it possible to work in the presence of the matrix interference without eliminating the interference itself. Indeed, the concentration of the analyte in the sample solution is detected accurately by conducting the concentration calibration in the presence of the matrix interference. The method of standard additions is schematically illustrated in Figure A-2.

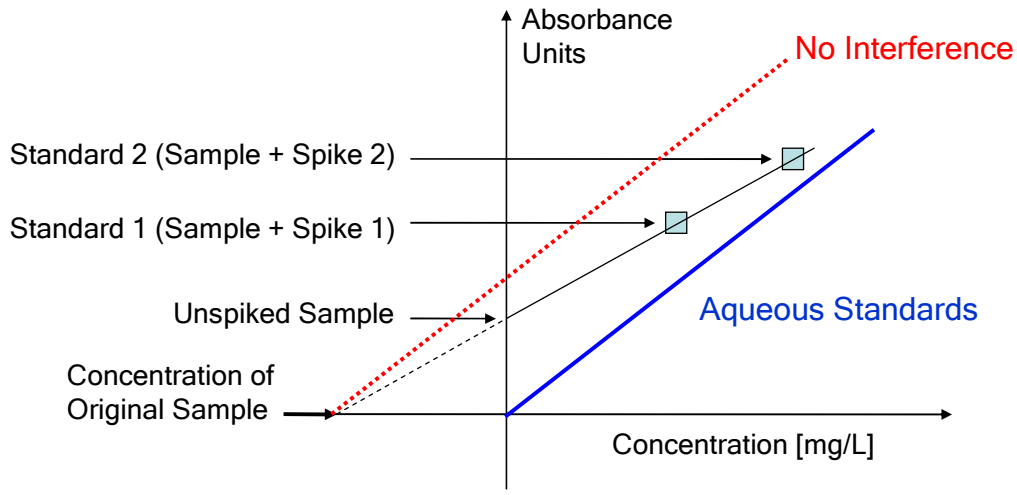

Figure A-2: The method of standard additions

The solid line passing through the origin in Figure A-2 represents a typical calibration line for a set of aqueous standards, where the zero absorbance is defined with DI water

blank. According to the aqueous standards calibration curve (Figure A-2), the absorbance increases linearly as the concentration of analyte increases. In the case of method of standards additions, the aliquots of a standard (spike solution) are added to portions of the sample (unspiked sample) in order to allow any interferent present in the sample to also affect the standard similarly. All portions are diluted to the same volume so that the final concentrations of the original sample (unspiked sample) constituents are the same in each case. Thus, only the amount of added standard (spike solution) differs by a known amount. It should be also noted that the absorbances for all the spiked solutions must fall within the linear portion of the working curve (aqueous standards calibration curve given in Figure A-1) for the method of standard additions to be used accurately.

As shown by the dotted line in Figure A-2, a plot of measured absorbance versus the concentration of added standard would be parallel to the aqueous standard calibration curve (i.e., Figure A-1) if there were no interference present in this sample, and offset by an absorbance value resulting from the analyte present in the unspiked sample. In the case of the matrix interference, both the number of ground state atoms producing atomic absorption and the absorbance from the analyte in the unspiked sample will be affected. Since the concentration of interference is the same in each solution (spiked samples), the change of the increase in the absorbance from each added standard will be by the same proportional amount. Therefore, a straight line will still result, but because of the interference, its slope, solid line with squares in Figure A-2, will be different from that observed for the aqueous standards.

In the presence of the matrix interference, the slope determined by the method of standard additions (solid line with squares in Figure A-2) is used as the calibration slope. An accurate determination of the sample concentration can still be made by continuing the concentration calibration on the abscissa backward from zero and extrapolating the calibration line backward until it intercepts the concentration axis. The value read on the concentration axis is taken as the concentration responsible for the absorbance of the unspiked sample. The procedure is repeated for all the samples.

The matrix interference was checked for both Pd and Ag plating solutions via the method of standard additions, as shown in Figure A-3[a] and Figure A-3[b], respectively.

Both for the Pd and Ag, the calibration slopes determined by the method of standard additions were found to be parallel to the slope of the calibration curve for the aqueous standards within the linear range where the Beer's law was applicable.

The results shown in Figure A-3 indicated that the AA flame analysis of the electroless Pd and Ag solutions was not affected by the interferences from the sample matrix, in which the linear calibration curve for the aqueous standards, shown in Figure A-1, can be effectively utilized to determine the Pd and Ag metal concentrations in the solution.

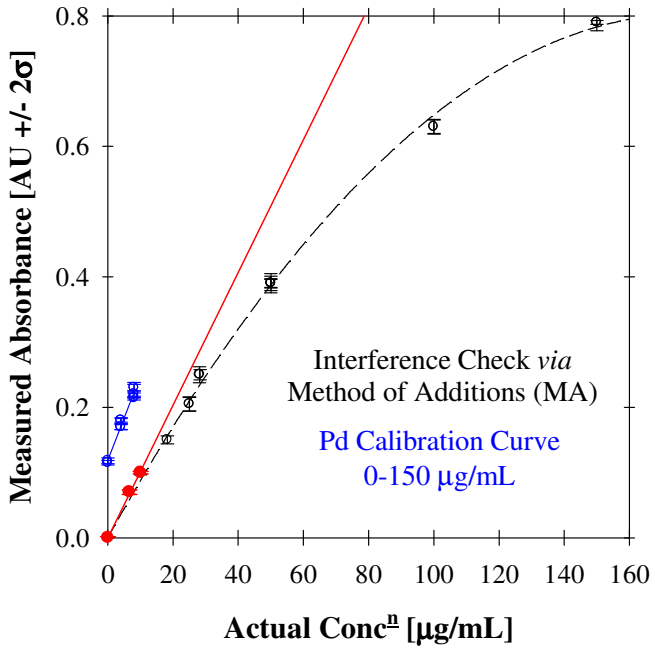

[a].

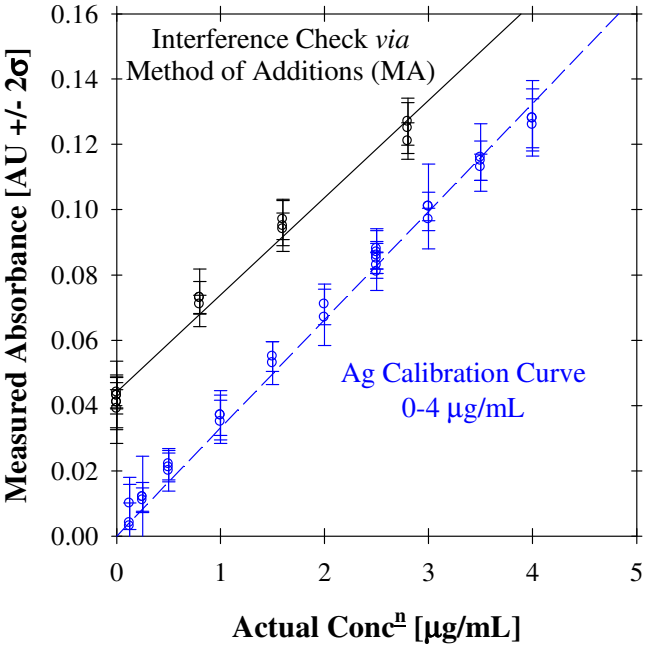

[b].

Figure A-3: Interference check via the method of standard additions for [a]. Pd and [b]. Ag plating solutions

Appendix B

B.1. Modeling Studies for Hydrogen Transport through Composite Pd and Pd/Ag Alloy Membranes

For the measurements reported at a temperature of 500°C, the H_2 permeance data listed in Table 2-8 for the composite Pd membranes formed by the electroless plating are plotted in Figure B-1.

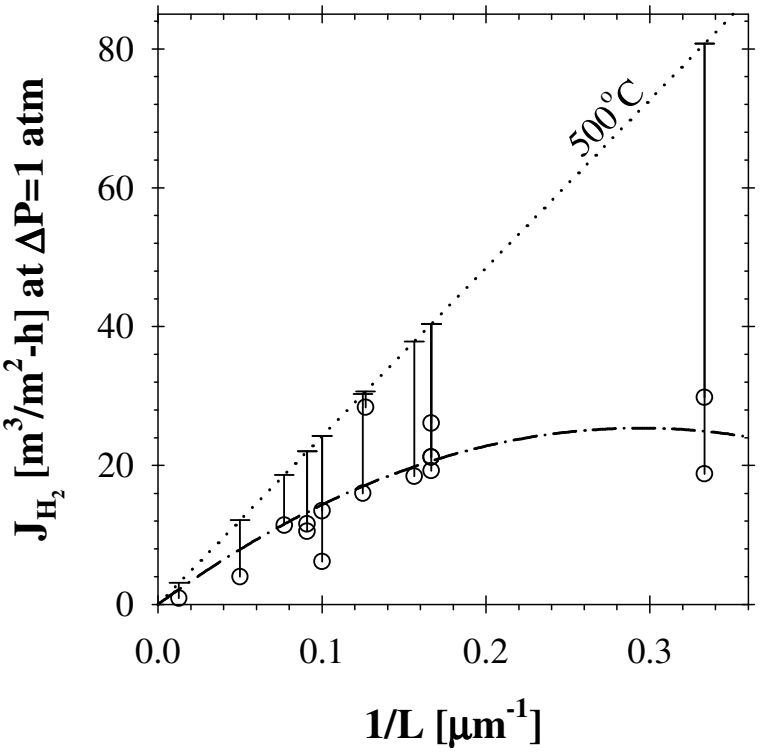

Figure B-1: H_2 permeation flux vs. inverse thickness plot for the composite Pd membranes listed in Table 2-8 at 500℃ and a trans-membrane pressure difference of 1 atm (dotted line shows the calculated H_2 flux for the Pd foil based on Equation (4-14). Error bars indicate the difference between the calculated permeation flux and that of measured value)

It should be noted that the H_2 permeation data for the composite Pd membranes listed in Table 2-8 were reported with n-values different from 0.5 indicating the possibility of either surface reactions or the diffusion of hydrogen atom in the bulk of the membrane layer as the rate-limiting step. In this respect, the summary plot in Figure B-1 compares the hydrogen permeation flux at 500°C and a fixed trans-membrane pressure of 1 atm (P_{shell} = 2 atm and P_{tube} = 1 atm). Indeed, the dotted line in Figure B-1 shows the calculated H_2 flux for the Pd foil using Equation (4-14) at the reported thickness, whereas the error bars indicate the difference between the calculated permeation flux and that of the measured value. As can be depicted in Figure B-1, the deviation from the theoretical H_2 flux is more pronounced as the thickness of the Pd layer decreases, indicating the significance of the likelihood mass transfer resistance exerted by the porous supports.

In fact, several studies in the literature have been devoted to understand the mass transfer effects and the modeling of the H_2 transport mechanism through composite Pd and Pd/alloy membranes (Itoh *et al.*, 1995; Ward and Dao, 1999; Goto *et al.*, 2000; Prabnu *et al.*, 2000; Basile *et al.*, 2001; Lin and Rei, 2001; Thomas, 2001; Elkina and Meldon, 2002; Hou and Hughes, 2002; Adrover *et al.*, 2003; Hou and Hughes, 2003; Lin *et al.*, 2003).

Although it seems unlikely that the external mass transfer effects can be completely eliminated for a 1 μm thick Pd layer due to the high H_2 permeation flux values that can be achieved theoretically, mass transfer limitations can possibly be minimized especially on the high pressure side (shell-side) of the membrane for Pd films below 10 μm (Ward and Dao, 1999). While applying vacuum on the downstream side of a Pd membrane can be effectively used to minimize and/or eliminate the external mass transfer resistance on the high pressure side, it is not practical in the presence of a porous support, where transport through the support is achieved by a combination of Knudsen diffusion and viscous (Poiseuille) flow, often termed as the slip-flow mechanism (Mardilovich *et al.*, 1998a).

Since the diffusion of gases (i.e., He, H_2, etc.) is strongly dependent upon the diameter of the pores, the mean pore size and the pore size distribution of the porous supports play an important role in defining the Knudsen and viscous (Poiseuille) flow

regimes. The mean free path of a molecule is defined as the average distance a gas molecule travels before it collides with another gas molecule, as shown in Equation (B-1):

$$\lambda = \frac{3.2\mu}{P}\sqrt{\frac{RT}{2\pi M}} \qquad (B\text{-}1)$$

Where λ is in m, μ is viscosity in Pa.s, P is pressure in N/m^2, T is temperature in Kelvin, M is the molecular weight in kg/kmol and R is the universal gas constant in 8.314x10^3 N-m/kmol-K. When the mean free path of a molecule is large compared to the pore diameter of the porous media, gas molecules collide with the wall and the molecule-wall collisions become important and lead to the "Knudsen diffusion" term, where Knudsen diffusivity is usually defined as the product of the average pore radius and the mean molecular velocity for the diffusing component. From the kinetic theory of gases, the mean molecular velocity in m/s is given as:

$$\bar{v} = \sqrt{\frac{8RT}{\pi M}} \qquad (B\text{-}2)$$

On the other hand, viscous (Poiseuille) flow dominates when the pore diameter is larger than the mean free path of the molecule, in which the gas acts as a continuum fluid driven by a pressure gradient, and molecule-molecule collisions take over molecule-wall collisions. By including the porosity and tortuosity to account for the actual diffusion in porous media, the flux for the combined Knudsen and viscous flow regimes is expressed as follows:

$$J_{\sup port} = \left(\frac{2}{3}\sqrt{\frac{8}{\pi}}\frac{\left(\frac{\varepsilon}{\tau}\right)r}{L_s\sqrt{RTM}} + \frac{1}{8}\frac{\left(\frac{\varepsilon}{\tau}\right)r^2}{L_s\mu(T)RT}P_{ave.} \right)\Delta P \qquad (B\text{-}3)$$

Where ε is the porosity, τ is the tortuosity, r and L_s are the average pore radius and the wall thickness of the support in meters, respectively, $P_{ave.}$ is the average pressure in atm and ΔP is the trans-membrane pressure in atm. As shown in Equation (B-3), support resistance can be minimized by the use of highly permeable tubes with high

porosity, large pores and reduced wall thickness without compromising the mechanical properties. Indeed, mass transfer at the low pressure side of the support can be enhanced by the use of a sweep gas to allow better mixing and cross-flow (Ward and Dao, 1999).

At steady state, H_2 permeation flux through the Pd layer, J_{H_2-Pd}, is equal to the H_2 flux through the porous metal support, $J_{H_2-Support}$, as schematically illustrated in Figure B-2. Therefore, Equations (4-9) and (B-3) can be exploited to quantify the effect of pressure drop and the support resistance on the H_2 permeation flux for composite Pd and Pd/alloy membranes(Thomas, 2001; Hou and Hughes, 2003; Guazzone, 2005).

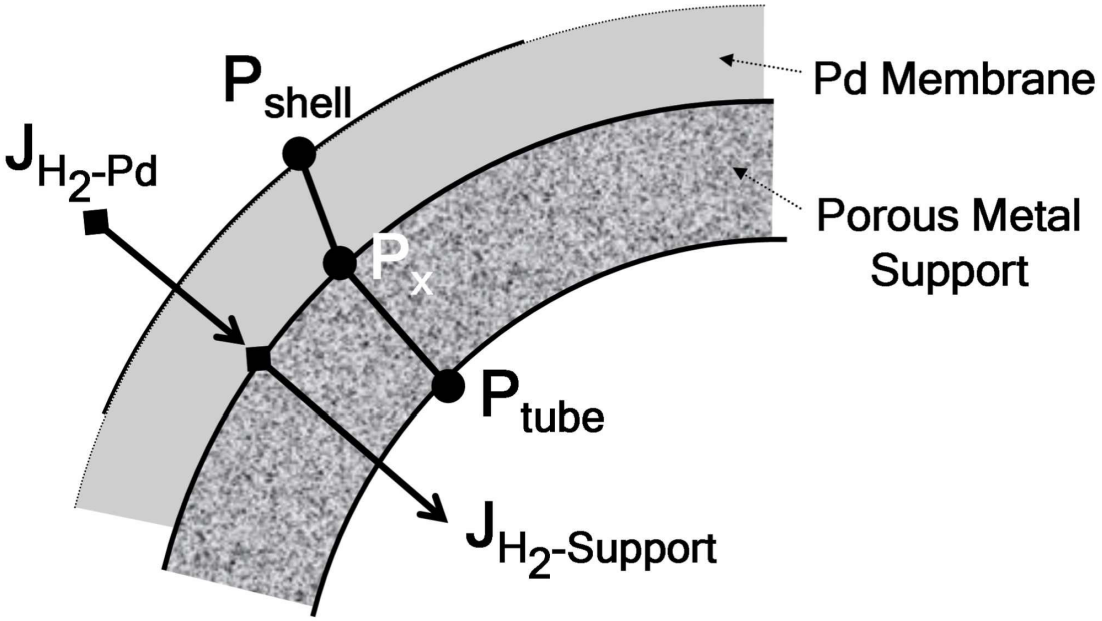

Figure B-2: Schematic for the H_2 transport through a composite Pd membrane

After correcting for the pressure terms in Figure B-2, as well as hydrogen gas and temperature corrections for the Knudsen and viscous (Poiseuille) regimes and substituting Equation (4-14) for the average H_2 permeability, Equations (4-9) and (B-3) transform into the following model equations, respectively:

$$J_{H_2-Pd} = \frac{Q_{Pd}(T)}{L_{Pd}}\left(P_{shell}^{0.5} - P_x^{0.5}\right) = \frac{6322.7e^{-\frac{15630}{RT}}}{L_{Pd}}\left(P_{shell}^{0.5} - P_x^{0.5}\right) \quad (B\text{-}4)$$

$$\begin{aligned} J_{H_2-Support} &= \left[\alpha_K(T_0) + \beta_v(T_0)\left(\frac{P_x + P_{tube}}{2}\right)\right](P_x - P_{tube}) \\ &= \left[\alpha_K(T_0)\sqrt{\frac{T_0}{T_x}}\sqrt{\frac{M_{He}}{M_{H_2}}} + \beta_v(T_0)\left(\frac{\mu_{He}(T_0)}{\mu_{He}(T_x)}\cdot\frac{T_0}{T_x}\right)\left(\frac{\mu_{He}(T_x)}{\mu_{H_2}(T_x)}\right)\left(\frac{P_x + P_{tube}}{2}\right)\right](P_x - P_{tube}) \end{aligned} \quad (B\text{-}5)$$

Where, T_0 and T_x are the reference (i.e, 293 K) and target temperatures in Kelvin, respectively. The Knudsen and viscous flow parameters $\alpha_K(T_0)$ in m^3/m^2-h-atm and $\beta_v(T_0)$ in m^3/m^2-h-atm^2, can be estimated from the intercept and slope of the He permeance vs. average pressure plot for the porous support at the reference temperature, T_0, respectively. The temperature dependence of the viscosity for He and H_2 gases are given in Equations (B-6) and (B-7), respectively (Perry and Green, 1997):

$$\mu_{He}(T_i) = 4x10^{-8}T_i + 7x10^{-6} \quad (B\text{-}6)$$

$$\mu_{H_2}(T_i) = 2x10^{-8}T_i + 4x10^{-6} \quad (B\text{-}7)$$

Where both μ_{He} and μ_{H_2} are in Pa.s and T_i is in Kelvin.

Hence, Equations (B-4) and (B-5) can be solved sequentially in order to estimate the unknown interface pressure, P_x, over a wide range of temperature, shell and tube side pressure and Pd film thickness, to elucidate the effect of support resistance on the H_2 permeation flux.

A more simplistic approach, based on the overall transport resistance, can be formulated by assuming that the H_2 transport through the composite membrane is governed by the additive resistances exerted by the Pd film and the porous support. In this respect, $P_x^{0.5}$ and P_x in Equations (B-4) and (B-5) are simply replaced by $P_{tube}^{0.5}$ and P_{shell}, respectively, and the actual H_2 permeation flux for the Pd film supported on a porous substrate can be directly estimated by using the following expression:

$$J^*_{H_2} = \left(\frac{1}{J_{H_2-Pd}} + \frac{1}{J_{H_2-Support}} \right)^{-1} \qquad (B\text{-}8)$$

The mass transfer and the resistance models given in Equations (B-4) and (B-8), respectively, were used to predict the H_2 permeance and the pressure drop across the membrane layer and the support tube in order to assess the possible contribution of the mass transfer resistance to the overall H_2 permeation resistance. The sample calculations were based on the room temperature He permeance of a 0.1 μm media grade Inconel support as shown in Figure B-3. Th Knudsen and the viscous flow parameters $\alpha_K(T_0)$ and $\beta_v(T_0)$ used in Equation (B-5) were 147 m^3/m^2-h-atm and 68 m^3/m^2-h-atm^2, respectively (also shown in Figure B-3).

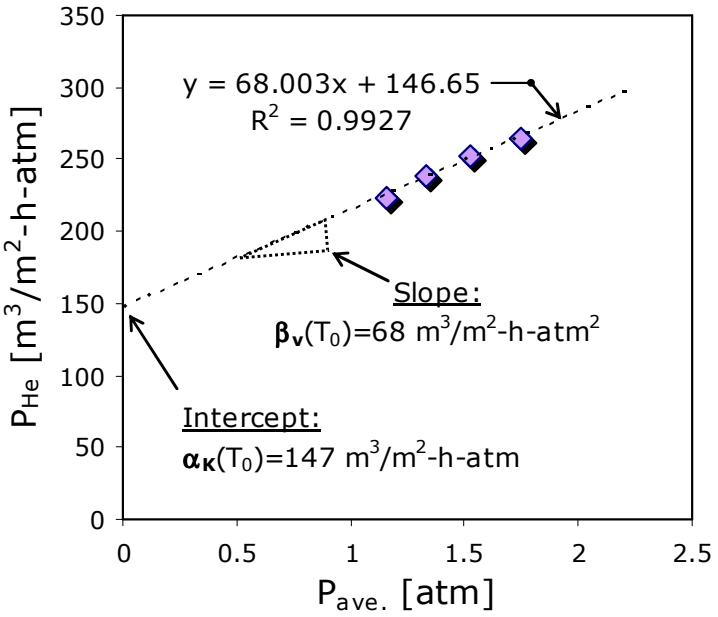

Figure B-3: Plot of He Permeance vs. $P_{ave.}$ for the 0.1 μm media grade Inconel Support at 20°C

Figure B-4 shows the H_2 permeance predictions for the Pd layers of different thicknesses supported on an Inconel tube, at 500°C and a trans-membrane pressure difference of 1 atm. As can be depicted in Figure B-4, both the mass transfer (full diamonds) and the resistance (full circles) model predictions for the H_2 permeance in composite Pd membranes were in good agreement. The error bars in Figure B-4 indicate the difference between the calculated and the predicted H_2 permeance for the Pd-foil

(based on Equation (4-14)) and the composite Pd membrane (according to model equations in (B-4) and/or (B-8)), respectively.

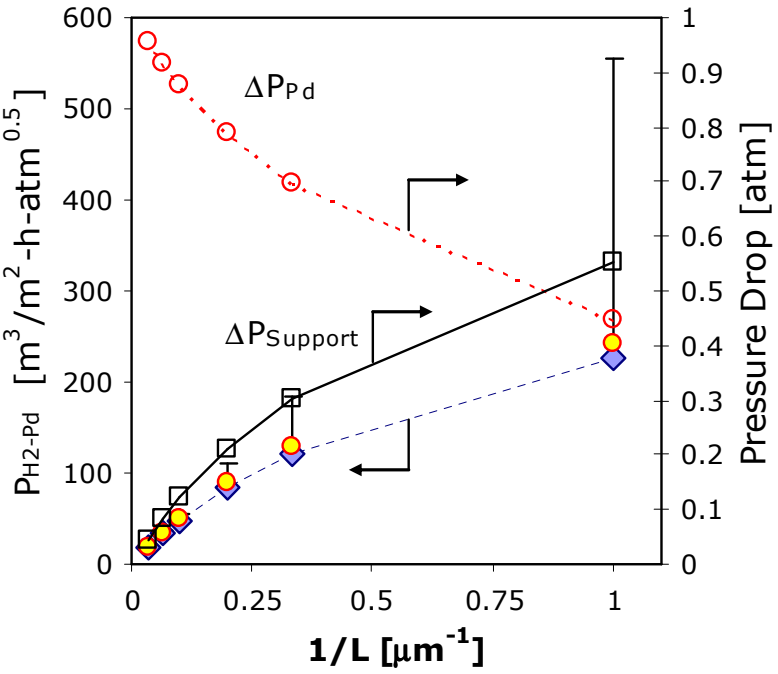

Figure B-4: Plots of H_2 permeation flux (left y-axis) and pressure drop (right y-axis) vs. inverse thickness at 500℃ and a ΔP of 1 atm (Full diamonds and circles are the H_2 permeance estimated from the mass transfer and the resistance models, respectively. Error bars indicate the calculated H_2 permeance for thePd-foil based on Equation (4-14) at 500℃ and a ΔP of 1 atm. Empty circles and squares are the pressure drop through the Pd-layer and support, respectively)

The pressure drop across the support increased with the decreasing Pd layer thickness, as shown in Figure B-4. Indeed, the difference between the calculated and the predicted permeance became significantly larger for the thin Pd membranes as the mass transfer resistance exerted by the Inconel support increased.

For a 7 μm thick composite Pd membrane, the model predictions at different temperatures and a trans-membrane pressure difference of 1 atm are shown in Figure B-5. Similarly, as the temperature increased, the pressure drop across the support increased and the mass transfer resistance became significantly larger at higher temperatures. Since the H_2 permeance is expected to increase with temperature, the deviation between the calculated and the predicted permeance increased at higher temperatures due to the presence of mass transfer resistance as can be depicted in Figure B-5.

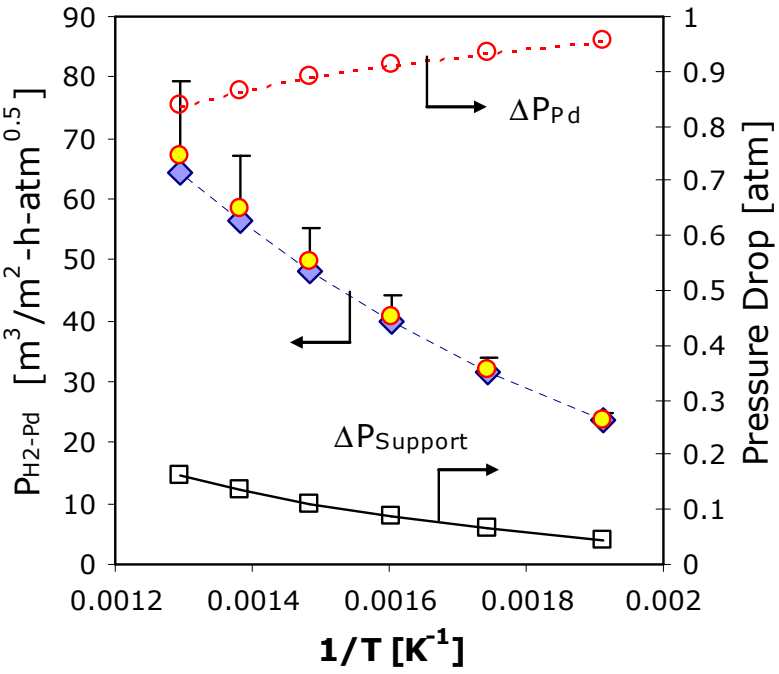

Figure B-5: Plots of H_2 permeation flux (left y-axis) and pressure drop (right y-axis) vs. inverse temperature for a 7 µm Pd layer at a ΔP of 1 atm (Full diamonds and circles are the H_2 permeance estimated from mass transfer and the resistance models, respectively. Error bars indicate the calculated H_2 flux for a 7 µm Pd-foil based on Equation (4-14) at a ΔP of 1 atm. Empty circles and squares are the pressure drop through the Pd-layer and support, respectively)

Both the mass transfer and the resistance models are of great importance for understanding the H_2 transport through composite Pd membranes and can be easiliy used to compare H_2 permeances at different temperatures, pressures and for membrane layers with different thicknesses.

Appendix C

C.1. Methodology for the Multiphase Quantitative Phase Analysis

XRD quantitative phase analysis is based on the fact that the intensity of the diffraction pattern of a particular phase in a mixture of phases depends on the concentration of that particular phase in the mixture (Cullity and Stock, 2001). However, the relation between intensity and concentration is generally non-linear. The diffracted intensity depends mainly on the absorption coefficient of the mixture, which varies with concentration. The basic equation for the diffracted intensity of a single phase in a diffractometer can be used as the starting point to find the relation between diffracted intensity and concentration, as shown in Equation (C-1).

$$I_{hkl} = \left(\frac{I_o \lambda^3 A_b}{32\pi r}\right)\left[\left(\frac{\mu_o}{4\pi}\right)^2 \frac{e^4}{m^2}\right]\left(\frac{1}{v^2}\right)\left[|F|^2 p\left(\frac{1+\cos^2 2\theta}{\sin^2\theta\cos\theta}\right)\right]\left(\frac{e^{-2M}}{2\mu}\right) \qquad (C\text{-}1)$$

Here:

I_{hkl} is the integrated intensity per unit length of diffraction line in J/m-s, I_o is the intensity of incident beam in J/m^2-s, λ is the wavelength of incident beam in m (1.5406 Å for CuK$_\alpha$ radiation), A_b is the cross-sectional area of incident beam in m^2, r is the radius of diffractometer circle in m, μ_o is equal to $4\pi*10^{-7}$ in kg-m/C^2, e is the charge on electron in Coulombs, m is the mass of electron in kg, ν is the volume of the unit cell in m^3 or Å^3, θ is the Bragg angle in radians, $F_{(hkl)}$ is the structure factor for reflection *hkl*, which equals to 4 times to that of the atomic scattering factor (F=4f) for the FCC unit cell and f is the atomic scattering factor, which is equal to $a*(\sin\theta/\lambda)^2+b*(\sin\theta/\lambda)+c$, where a, b and c are constants. For Pd, Ag and Pd/Ag (23 wt% Ag), the atomic scattering factor relationships takes the following forms:

$f_{Pd} = 23.731*(\sin\theta/\lambda)^2-57.428*(\sin\theta/\lambda)+47.207$

$f_{Ag} = 23.377*(\sin\theta/\lambda)^2-56.459*(\sin\theta/\lambda)+46.179$

$f_{Pd77Ag23} = 23.458*(\sin\theta/\lambda)^2-57.205*(\sin\theta/\lambda)+46.971$

Furthermore, in Equation (C-1), *p* is the multiplicity factor and equal to 8 for cubic systems (hhh=8), $[1+\cos^2 2\theta]/[\sin^2\theta*\cos\theta]$ is the Lorentz-Polarization factor, μ is the linear absorption coefficient in m^{-1}, μ/ρ is the mass absorption coefficient in cm^2/g, ρ is the density of the metal in g/cm^3 and e^{-2M} is the temperature factor, which is given by:

$$M = \frac{11500T(K)}{MW.\Theta_i^{\,2}}.\left[\Phi_X + \frac{\Theta_i}{T(K)/4}\right].\left(\frac{\sin\theta}{\lambda}\right)^2 \qquad (C\text{-}2)$$

where, Θ is the Debye characteristic temperature of the substance in K, with

$\Phi_{X=[\Theta/T(K)]} = -0.0014[\Theta/T(K)]^3 + 0.0302[\Theta/T(K)]^2 - 0.2507[\Theta/T(K)] + 0.9992$

Some of the physical properties to be used in DCM calculations for the Pd, Ag and the Pd/Ag-Alloy phases are summarized in Table C-1.

Table C-1. Physical properties for Pd. Ag and $Pd_{77}Ag_{23}$ used in DCM calculations

	μ/ρ [cm^2/g]	ρ [g/cm^3]	μ [m^{-1}]	$\lambda_{CuK\alpha}$ [Å]	a [Å]	ν [$Å^3$]	Θ [K]	MW [g/gmol]
Pd	207	12.02	24.8814	1.5406	3.8896	58.85	275	106.4
Ag	223	10.5	23.415	1.5406	4.0855	68.19	210	107.9
$Pd_{77}Ag_{23}$	210.68	11.67	24.5872	1.5406	3.9347	60.91	260.05	106.7

XRD direct comparison method (DCM) can be directly applied to polycrystalline aggregates and has been widely used since its development by Averbach and Cohen (1948) to measure the amount of retained austenite in hardened steel. The methodology is quite trivial and proceeds by expressing the basic intensity equation as follows (Cullity and Stock, 2001):

$$K = \left(\frac{I_o\lambda^3 A_b}{32\pi r}\right)\left[\left(\frac{\mu_o}{4\pi}\right)^2 \frac{e^4}{m^2}\right] \qquad (C\text{-}3)$$

and

$$R_i = \left(\frac{1}{v^2}\right)\left[|F|^2 p\left(\frac{1+\cos^2 2\theta}{\sin^2\theta\cos\theta}\right)\right]\left(e^{-2M}\right) \qquad (C\text{-}415)$$

The diffracted intensity equation is then given by:

$$I = \frac{KR_i}{2\mu} \qquad (C\text{-}5)$$

where, ***K*** is a constant and independent of the kind and amount of the diffracting substance and $\boldsymbol{R_i}$ depends on θ, hkl and the kind of substance. In order to analyze a mixture of phases, Equation (C-5) can be rewritten for each particular diffraction line of the existing phases in the mixture by substituting μ_{mix}, the linear absorption coefficient of the mixture, for μ and multiplying with the corresponding volume fraction of the particular phase.

$$I_{Ag} = \frac{KR_{Ag}C_{Ag}}{2\mu_{mix}} \qquad (C\text{-}6)$$

$$I_{Pd} = \frac{KR_{Pd}C_{Pd}}{2\mu_{mix}} \qquad (C\text{-}7)$$

$$I_{PdAg} = \frac{KR_{PdAg}C_{PdAg}}{2\mu_{mix}} \qquad (C\text{-}8)$$

The constants K and μ_{mix} are eliminated by dividing against a reference phase (i.e., Ag) and re-arranged to obtain the following relationships for Pd and Pd/Ag phases:

$$C_{Pd} = \frac{R_{Ag}C_{Ag}I_{Pd}}{R_{Pd}I_{Ag}} \qquad (C\text{-}9)$$

$$C_{PdAg} = \frac{R_{Ag}C_{Ag}I_{PdAg}}{R_{PdAg}I_{Ag}} \qquad (C\text{-}10)$$

Once C_{Pd} and C_{PdAg} are found, the value of C_{Ag} can be obtained from an additional relationship:

$$C_{Ag} + C_{Pd} + C_{PdAg} = 1 \qquad (C\text{-}11)$$

Substituting Equations (C-9) and (C-10) into Equation (C-11) and rearranging, we get;

$$C_{Ag} = \frac{1}{\left[1 + \frac{R_{Ag} I_{PdAg}}{R_{PdAg} I_{Ag}} + \frac{R_{Ag} I_{PdAg}}{R_{PdAg} I_{Ag}}\right]} \qquad (C\text{-}12)$$

Finally, the weight fractions are calculated using the known densities of the respective metal phases.

Appendix D

D.1. Emprical Rate Laws and Stoichiometry

Chemical kinetics is used to predict the rates of chemical reactions and to delineate the path or paths by which the reactants proceed to products. The dependence of the reaction rate on the concentrations of the species that participate in the reaction is almost without exception determined through experimental observation at several temperatures and initial concentrations of the reactants (Fogler, 1992). The theoretical expression used to relate the dependence of the reaction rate to the concentrations of reactants and products, also called the differential rate law, is defined in the following differential form:

$$Rate = -r_i = \pm\frac{dC_i}{dt} = k(T)f\left[C_{A_i}^{\alpha}, C_{B_i}^{\beta}C_{C_i}^{\gamma}...\right] \qquad (D\text{-}1)$$

where $\pm\frac{dC_i}{dt}$ is the rate of disappearance or the formation of the ith species, which is positive for the products and negative for the reactants, $k(T)$ is the temperature-dependent reaction rate constant, C_i is the time-dependent concentration and the exponents $\alpha, \beta, \gamma...$ are the reaction orders for the respective species. The temperature dependence of the reaction rate constant is expressed by the Arrhenius equation:

$$k(T) = Ae^{-\frac{E_a}{RT}} \qquad (D\text{-}2)$$

where A is the pre-exponential or frequency factor, E_a is the activation energy in J/mol, R is the universal gas constant and T is the temperature in Kelvin.

The reaction orders, $\alpha, \beta, \gamma...$, can only be determined from the reaction stoichiometry in the special case of an elementary reaction, in which the reaction takes place with a mechanism implied by the reaction stoichiometry. In general, the order of

the reaction with respect to the concentration of each reactant is found experimentally to determine the differential rate law. For the electroless plating reactions of Pd and Ag, the differential rate law in Equation (D-1) takes the following form:

$$Rate = -r_A = -\frac{dC_A}{dt} = k(T)C_A^{\alpha}C_B^{\beta}C_C^{\gamma} \qquad (D\text{-}3)$$

Furthermore, Table D-1 shows the stoichiometric relationships derived for the electroless plating reactions of Pd and Ag shown in Equations (10-2) and (10-3), respectively.

Table D-1. Stoichiometric table for a reaction of type aA+bB+cC → dD+eE+fF+gG

Species	Initially (mol)	Change (mol)	Remaining (mol)
A	N_{A_0}	$-N_{A_0}X$	$N_A = N_{A_0}(1-X)$
B	N_{B_0}	$-\frac{b}{a}N_{A_0}X$	$N_B = N_{A_0}\left(\Theta_B - \frac{b}{a}X\right)$
C	N_{C_0}	$-\frac{c}{a}N_{A_0}X$	$N_C = N_{A_0}\left(\Theta_C - \frac{c}{a}X\right)$
D	N_{D_0}	$+\frac{d}{a}N_{A_0}X$	$N_D = N_{A_0}\left(\Theta_D + \frac{d}{a}X\right)$
E	N_{E_0}	$+\frac{e}{a}N_{A_0}X$	$N_E = N_{A_0}\left(\Theta_E + \frac{e}{a}X\right)$
F	N_{F_0}	$+\frac{f}{a}N_{A_0}X$	$N_F = N_{A_0}\left(\Theta_F + \frac{f}{a}X\right)$
G	N_{G_0}	$+\frac{g}{a}N_{A_0}X$	$N_G = N_{A_0}\left(\Theta_G + \frac{g}{a}X\right)$
I (inerts)	N_{I_0}	-	$N_I = N_{A_0}\Theta_I$
Total	N_{T_0}	→	$N_T = N_{T_0} - \delta N_{A_0}X$

Where N_{i0} is the initial moles of species *i*, N_i is the moles of species *i* at time t, X is the conversion or the yield of reaction, Θ_i is the initial mole ratio of the species *i* with respect to species *A* and expressed as $\Theta_i = \frac{N_{i_0}}{N_{A_0}} = \frac{C_{i_0}}{C_{A_0}} = \frac{y_{i_0}}{y_{A_0}}$ and δ is the stoichiometric

constant given as $\delta = \frac{g}{a} + \frac{f}{a} + \frac{e}{a} + \frac{d}{a} - \frac{c}{a} - \frac{b}{a} - 1$. C_{i_0} is the initial concentration of species *i*, which is the number of moles per unit volume, V. Since $V = V_0$ in a constant-volume batch reactor, the concentration of species *i* is defined as $C_{i_0} = \frac{N_{i_0}}{V} = \frac{N_{i_0}}{V_0}$. Therefore, the concentration of the species in Equation (D-3) can be expressed as follows:

$$C_A = \frac{N_A}{V_0} = \frac{N_{A_0}(1-X)}{V_0} = C_{A_0}(1-X) \qquad \textit{(D-4)}$$

$$C_B = \frac{N_B}{V_0} = \frac{N_{A_0}\left(\Theta_B - \frac{b}{a}X\right)}{V_0} = C_{A_0}\left(\Theta_B - \frac{b}{a}X\right) \qquad \textit{(D-5)}$$

$$C_C = \frac{N_C}{V_0} = \frac{N_{A_0}\left(\Theta_C - \frac{c}{a}X\right)}{V_0} = C_{A_0}\left(\Theta_C - \frac{c}{a}X\right) \qquad \textit{(D-6)}$$

The rate law in Equation (D-3) takes the following form after substituting Equations (D-4), (D-5) and (D-6):

$$-r_A = -\frac{dC_A}{dt} = k(T)\left[C_{A_0}(1-X)\right]^{\alpha}\left[C_{A_0}\left(\Theta_B - \frac{b}{a}X\right)\right]^{\beta}\left[C_{A_0}\left(\Theta_C - \frac{c}{a}X\right)\right]^{\gamma} \qquad \textit{(D-7)}$$